# Flatness measurements of CCDs

# and mosaics of CCDs

**Diplomarbeit**

from

Stefan Strőbele

supervised by

Prof. Dr. Bernhard Lau
at the
Fachhochschule Ulm

performed at the

European Southern Observatory
Optical detector team
Garching

April 1999

# Preface

Astronomy is a fascinating area of science, seeking to understand the size, structure and evolution of the universe. However, astronomy is limited by a fundamental constraint. By its nature, it is an observational science; astronomy is dependent upon receiving light from the rest of the universe. The amount of light received from distant galaxies is very small and thus astronomers are always seeking ways to more efficiently collect the faint signals from the heavens.

There are three ways to enhance the ability to observe faint objects: (1) building larger telescopes to collect more light – presently there is a major building "boom" of 8-10 meter telescopes, (2) producing more sensitive detectors to "capture" a higher percentage of the light – modern detectors now have over 90% efficiency, and (3) making larger detectors so that more objects can be observed at the same time, which makes the entire telescope system more efficient.

Astronomy makes use of all wavelengths of light, but in this thesis work, I concentrated on the detectors that are used to observe "optical" light, i.e. 300 – 1100 nm. These detectors, which are called Charge Coupled Devices (CCDs) have high efficiency and are now being made very large. But to be useful in an instrument, the light on a CCD must be in focus. To obtain good focus over the entire large CCD, the CCD must be very flat. Measuring the flatness of CCDs is not an easy task since high accuracy (3 microns) non-contact technique is required.

In this thesis, I describe a measuring system that I developed to make CCD flatness measurements.

I begin briefly by describing CCD detectors.

# 1. Introduction

A Charge Couple Device (CCD) is a detector of optical radiation made of silicon. When a light particle called a photon is absorbed in the CCD it can release a photoelectron. These liberated electrons can be collected in small areas and later be counted. The numbers of photoelectrons collected within each small area is proportional to the number of photons that were incident on the area. A CCD consists of a 2 dimensional array of small square areas (typically 15 *15 micron) which are called pixels. Each pixel is distinct from its neighbours and the electrons collected in each pixel can be counted individually. The image from the CCD consists of a matrix of numbers representing the intensity of light incident on the CCD. This matrix of brightness values is typically viewed on a computer screen.

Compared to a conventional photographic film CCDs have two main advantages:
(a) CCDs are much more sensitive than films (80% quantum efficiency versus 2-3% of film) and,
(b) the image of a CCD is digital and can be read directly into a computer, thus overcoming the large amount of labour involving in loading, processing and digitizing film.

To understand why CCDs must be very flat see the simplified presentation of the beam path of a telescope shown in *Figure 1*.

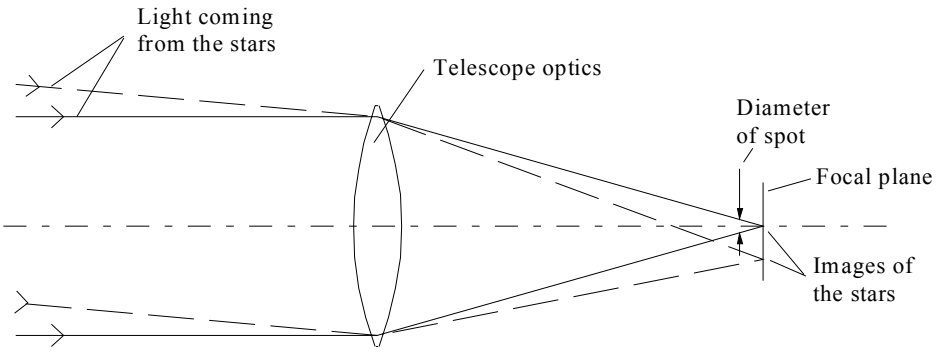


***Figure1**. Beam cone of a telescope. If the detector is not exactly in the focal plane the diameter of the image of a star on the detector increases.*

The parallel beams coming from a star get refracted by the telescope optics and converge at the focal plane. All beams coming from one star are concentrated into a small spot at the focal plane. On either side of focus, the star's diameter increases and the image blurs. Typically the depth of focus is between 18 and 50 microns.
High quality CCD detectors are now being procured with 2048 by 4096 square pixels, each 15 microns on a side. Compared with a high quality computer monitor

(1024*1024 pixels), this is equal to an image that covers 8 computer screen. As large as this may seem, astronomers desire even larger detectors for astronomical instruments. To achieve even larger focal planes, several CCDs are mounted into a mosaic, such as the 8192 by 8192 pixel mosaic used in ESO's Wide Field Imager. In this way it is possible to overcome the limited size of CCDs to build even larger detector focal planes. However, in a mosaic the detector surface is not completely filled. There are gaps and possibly steps between the devices and each device may be tilted differently.

The goal of my Diplomarbeit was to find a way to measure the flatness of individual CCDs and the misalignment of mosaicked CCDs so as to give the corrections for proper alignment.

# 2. Requirements for the flatness of optical detectors in Astronomy.

The tolerance for the deviation of the detector surface from the ideal image plane depends on the size of the pixels of the detector and the f-number of the instrument. The usual requirement is for the image blur to be less than the pixel size. This tolerance is given by multiplying the f-number and the pixel size. For an f/2 instrument with 15 micron pixels the CCD must be within ±30 micron. Some spectrographs have a much stricter requirement, such as half pixel blur limit.

## 2.1 Description of the CCD and its housing

The CCD surface and its optical properties are a critical issue for the measurement procedure and definition of appropriate technology. It is also important to know about the usage of the CCDs and the accessibility for measurement and alignment.

The image in Figure 2 shows a typical CCD detector in its dewar. The CCD sits behind the window on the top. The wires for operating the device and data readout are feed through the connectors around the upper part and connected to the external control unit. Underneath the CCD is the cooling system consisting of a tank for liquid nitrogen and a thermal connection from the nitrogen to the CCD. The detector is cooled to -90°C to -120°C in order to reduce dark current. For achieving good isolation between the cold parts and the outside, the dewar is evacuated to less than $1*10^{-5}$ mBar. Without a good vacuum, the thermal conductivity of the air inside the dewar would prevent the CCD from getting cold enough and the nitrogen consumption would increase dramatically.

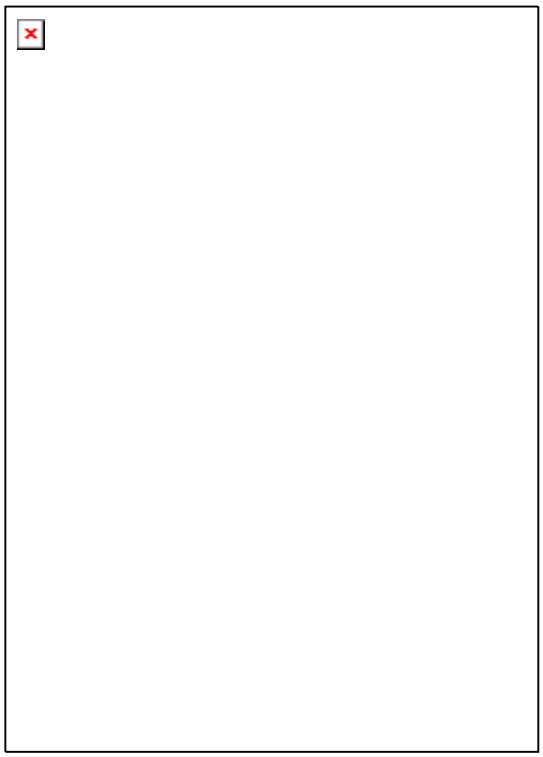

***Figure 2****. The picture shows a CCD in its dewar which is used to keep the CCD cool and hold the detector rigidly in place. The upper part contains the CCD, the wiring and the connectors. The cylinder attached below contains the cooling system and tank for liquid nitrogen.*

The dewar is mounted to the telescope and is moved with the telescope into many different orientations. This means that the CCD must be kept stable and the dewar must work in every position. Since it is important to know the planarity and mosaic alignment when the system is cold, it is essential to be able to measure through the window. The thickness of the window is up to 10 mm and the distance of the CCD from this window is also about 10 mm. This limits the variety of possible technologies for measuring the CCD flatness. Also avoid damage to the CCD surface we must use a non-contact method, thus we are limited to an optical based approach.

For all optical gauges, the property of the surface under test is a very critical issue. Thus, at this time we discuss the surface of CCDs.
In general there are two different kinds of CCDs. “Frontside” and “backside” devices. To understand the difference we a look to how they are manufactured. The basis for both types is a silicon waver on which the electrodes for the charge transfer are built during several steps of the CCD manufacturing. The electrodes have typically a

thickness 0.5 microns. If the CCD is illuminated from the side where the electrodes are (frontside), light gets absorbed by the electrodes and the quantum efficiency especially for short wavelengths is bad. To overcome this disadvantage some CCD manufacturer turn the waver after the electrodes on the front side are finished. The turned CCDs will then after additional manufacturing steps be illuminated at its backside. This prevents the absorption of the electrodes and makes it possible to reduce the amount of light reflected by the surface of the CCD by the usage of anti-reflection coatings. With this technology it is possible to achieve a quantum efficiency of up to 90% over a wide range of the spectrum of visible light.

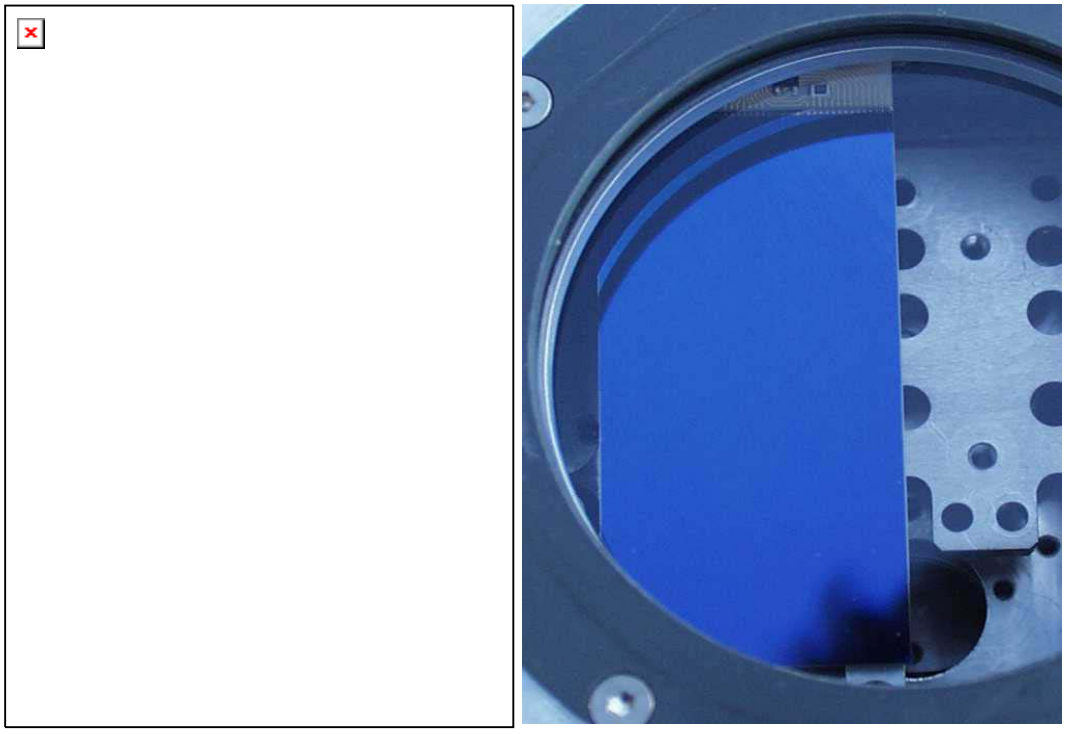

***Figure 3.*** *Image of a front side CCD (left). On the on its surface you can see structures of the electrodes used for charge transfer. The surface of a backside CCD (right) shows no structure looks like a dark, coloured mirror.*

Figure 3 shows frontside and backside CCDs. The frontside CCD, with the charge transfer electrodes on the illuminated side, has a matt appearance. Under illumination of some directions it shows diffraction effects due to the grating effect of the electrode structure.

The surface of the backside CCD is glossy and looks like a dark mirror. The colour of the reflection depends on the anti-reflection coating and varies from yellowish grey to intense blue. The reflectivity for some wavelengths is below 0.5%.

Since the manufacturers are now able to deliver high quality backside illuminated CCDs, the importance of front side devices is decreasing for astronomy. At the moment both kinds are used and should therefore be measurable.

Inside the dewar the CCDs are attached to a mounting plate with 3 screws with shims. The distance and tilt adjustment is done by correction of the thickness of shims between table and CCD. The proper thickness of these shims is the dimension which we have to determine. The accuracy achievable for this is critical and must match the requirements.

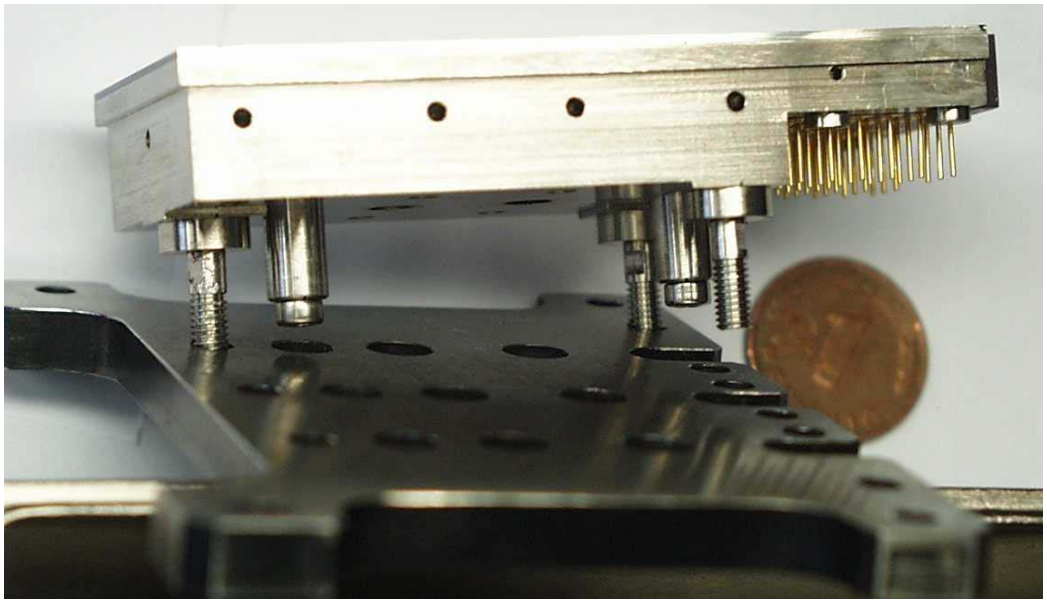

***Figure 4.*** *A CCD when it is assembled.*

Figure 4 shows the supporting plate of the CCD, the connector pins (right), and on the bottom of the CCD three threaded bolts used for attaching the CCD onto the carrier plate. The two rods (without thread) are for horizontal alignment of the CCD. After mounting the CCDs, the carrier plate is assembled in the dewar.

## 2.2 Requirements to measurement of the flatness.

The flatness requirement of the detectors determines the requirements of the of the measurement accuracy. A guideline for the accuracy the measuring instrument is that it should be 7 to 10 times more accurate than the acceptable flatness tolerance. Since the flatness of a single CCD should be ±15 micron and a mosaic of ±25 microns our goal is for a measurement accuracy of 3 microns. This is valid for the corrections to be

applied to the CCDs and not for a measurement of a single point. The mathematics used for getting the correction at the desired point will also have an influence. Therefore the number of 3 microns should be used only as a provisional accuracy goal which must be verified in more detail.

The size of the area have to be measured is determined by the dimensions of the largest mosaic camera in planning at ESO. It is the ΩCAM (Omegacam), a wide field imaging instrument with 16,384 by 16,384 pixels (15 micron square pixels) Taking into account the gaps between CCDs the mosaic will extend over 260 by 260mm. In addition, outside the mosaic will be several tracker CCDs. So a field of 300 by 300mm is the minimum field to be measured. Since we like to measure small tolerances only in the height (Z direction) the accuracy of the position (X, Y direction) of the single measurement plays a secondary role.

In addition to these numbers for accuracy and dimensions, we have the following specifications for the measuring device.

## 2.3 Summary of the requirements:

1. Accuracy in height (Z): 3 micron
2. Range of measurement in height (Z) > 1mm
3. Area measurable: 300mm * 300mm
4. Low accuracy in position (X, Y, 100 micron)
5. Frontside and backside CCDs (matt and glossy surfaces)
6. Reflectivity below 0.5%
7. Measurement through a dewar window (thickness 10mm with CCD 10mm behind the window)
8. Automated operation
9. Good reliability
10. Easy to handle and move
11. Flexible for usage at other applications (e.g. measuring machine parts)

And what is important for any measuring system, the result must be repeatable

Before presenting possible solutions and the solution I made for this diplomarbeit, I present the methods being used by other observatories for CCD flatness measurement.

# 3. State of art in measuring the flatness of CCD detectors at astronomical observatories.

## 3.1 ESO

Up to now ESO has used a very simple method to measure the flatness of CCDs. A microscope focused by eye on the surface of the CCD with the displacement of the microscope objective measured by a dial gauge. Moving the CCDs on a precision x-y stage and repeating this measurements at several positions on the CCD, the CCD topography, tilt and offset can be calculated.

Due to the short distance of the CCD of the microscope lens, these measurements can not be done with a window in front of the CCD. This poses a risk for contaminating the CCD with dust from the environment and accidental damage during measurement. There is also a subjectiveness of the person carrying out the measurement and some experience necessary to achieve repeatable results. And, as al the steps (positioning, focusing, recording) must be done manually this method is very time consuming.

## 3.2 University of California /Lick Observatory

At the Lick Observatory a more automated and advanced measuring system is used. They project a laser beam on the surface of the CCD and detect the deflection of the beam due to the tilt of the CCD. A diagram of the system in Fig.5 depicts the system geometry.

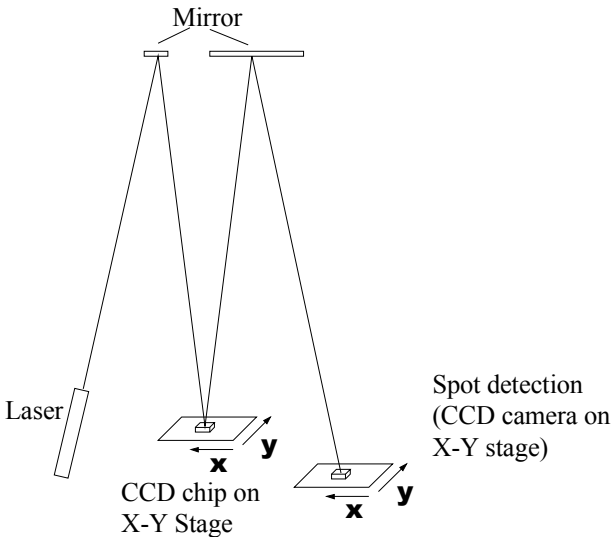


***Figure 5.*** *Diagram of the set up used for CCD flatness measurements used at the Lick Observatory and University of California. There is a laser spot directed by a mirror to the surface under test. The reflection hits a second mirror which point the beam to conventional camera, detecting the spot position. As the CCD is moved and the slope of its surface changes the camera records a movement of the spot. This movement is proportional to the slope of the surface and can therefore be used for the reconstruction of the surface of the CCD.*

The lick system consists of a laser an X-Y translation table on which the CCD will be put, two mirrors and a camera for detecting the position of the reflected laser beam. The laser beam is directed by the first mirror onto the CCD measured, then reflected at its surface to the second mirror directing the beam onto the spot detection system. This consists of a CCD camera mounted on a second X-Y table, in that way that this camera can follow the spot if it moves. The CCD under test is scanned by moving it, and if the local tilt of the CCD changes, the spot on the camera moves. By scanning over the whole surface and recording this movement, the topography of the CCD can be reconstructed.

One initial condition for characterising the topography of an object with this method is that its surface must be continous. This means that it is not possible to measure steps on a surface or between single CCDs of a mosaic. It requires also CCDs reflecting the beam without blurring it. For example if the spot on the camera gets to fuzzy it is difficult to exactly determine is position.

Since this system is not able to measure steps between the CCDs of a mosaic it will not be suitable for our purposes.

### 3.3 Royal Greenwich Observatory

At the Royal Greenwich Observatory (RGO) large efforts were made to be able to measure the flatness of CCD detectors. At the RGO a procedure based on the Hartman mask was developed.

In this system a lens and a mask with 2 holes out of the optical axis are used to project 2 convergent beam cones on a active CCD. By reading out the image of the CCD, there is only one spot in the image if the detector is exactly at the focal plan of the projection system.

If the CCD is outside of the focal plane there are two spots in the image. The distance between the two spots is proportional to the deviation of the detector surface to the focal plane.

To get a surface map of the CCD it is necessary to scan over the surface during one exposure, and detect the spot positions in the image, which gives the offsets at the positions. With this data the shape of the surface can be described.

In general this procedure delivers the distance of the detector surface to the optical system at a certain point. This is independent whether the surface is continuous or not. Thereby it is possible to measure the flatness of mosaics of CCDs with this system.

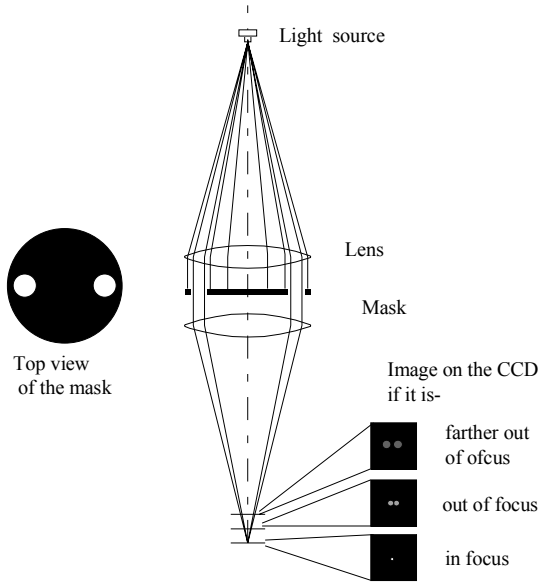


***Figure 6**. Optical schematic for the technique used by RGO for flatness measurement of CCDs*

Analysing the image data reveals an ambiguity. It is there not detectable whether the CCD surface is above the focal point or below it, if only the distance of the two points is used. If you take care that the whole surface is either above or below the focal point of the projection system this does not matter.

The disadvantage of this technique is that the CCD has to be active, which means that it have to be electrically connected and cooled down. Especially the cooling down takes a long time. This stretches the time needed for a correction cycle consisting of measuring the topography, correcting the tilts of the CCDs and measuring again by much. The analysis of the image data will require especially for large mosaics a fast computer and more dedicated software. Also, it will not be able to measure mechanical samples.

# 4. General possibilities for measuring the topography of CCDs and mosaics of them.

The measurement approaches used at other observatories do not satisfy all our requirements. Also these approaches are time intensive and it is useful to get a fast result to minimise the measurement, adjustment and remeasurement cycle. Therefore it is necessary to look for other possibilities for measuring CCD and mosaic flatness

## 4.1 Interferometry – Narrow bandpass

The most common technique for measuring topography of optical surfaces very accurately is interferometry. For our special application interferometry does not work since for reconstruction of the shape of the CCD a fringe pattern of very narrow banpass light is analysed.
Because of the gaps between the single CCDs the fringe pattern is interrupted and it is impossible to calculate a height difference between CCD. There will occur an uncertainty of an integer number of half wavelengths.

### 4.1.1 Scanning white light Interferometer

In general a white light interferometer can be used as a conventional Micheolson interferometer, as it is done by Institut fűr Laser in der Messtechnik Ulm (ILM).

A Michelson interferometer (Figure 7) consists of a light source creating a coherent beam, which is then divided by a beam splitter into two parts, the reference part and the signal part. The reference goes to a movable mirror, reflected back to the beam splitter and superimposed with the signal beam coming from the object under study. Along this beam you can observe interference. Such a system gives you very accurate information on the difference of the phase between both beams at a certain point and thereby of the difference of the surfaces of the reference mirror and the surface under test, but not an absolute distance to this surface.

The white light properties are important. White light in this context means light with a wide bandpass and a small coherence length. This has the consequence that there is constructive interference of the two beams only if the path length of both arms of the interferometer are equal within the coherence length of the light used.
Changing the path length of the reference arm to equalise the path in both arms it is possible to detect constructive interference. In the system used in Ulm the intensity of the combined beam is detected by a photo diode while the mirror in the reference path is shifted with continuous speed. As long the difference in the pathlengths is larger than the coherence length the diode detects a constant intensity, since no constructive interference occurs. If both arms are equal in length, constructive interference occurs at the photodiode. Due the continuous movement of the mirror, zones of constructive and destructive interference alternate at the position of photo diode of which then the fluctuation of intensity are recorded. At the same time the position of the mirror is measured. By using light with a coherent length of few microns, distance can be measured with the same accuracy by only detecting whether at a certain position of the reference mirror constructive interference is detectable. Analysing the frequencies and behaviour of the constructive interference it is possible to measure this distance with higher accuracy. The group in Ulm managed to reach accuracy of about 20 nm.

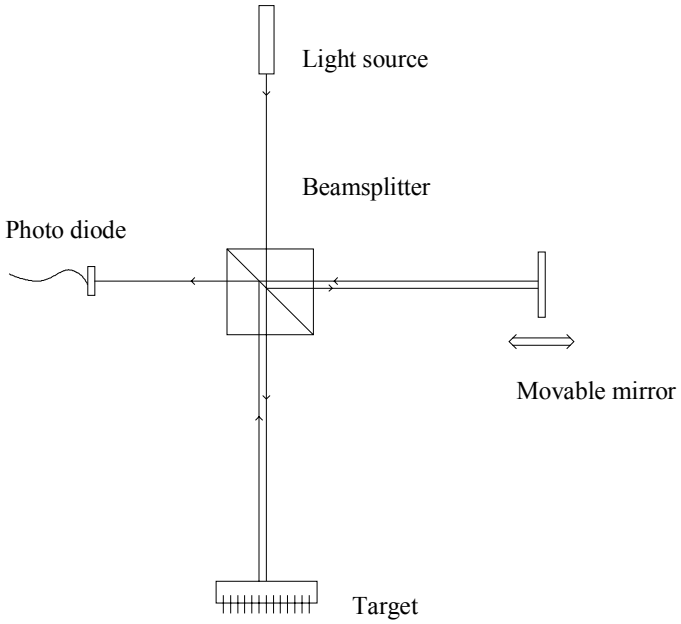


***Figure** 7. Scanning Michelson interferometer. The path length of the reference arm can be varied over a wider range (movable mirror) Since there is light with short coherence length used interference occurs at the photodiode only when both arms are equal in length. By measuring the position of the movable mirror the distance to the target may be determined.*

After a calibration of the pathlength of the reference arm it is possible to measure the absolute distance to the target. This can be done at several positions to be able to characterise a surface.

This procedure overcomes another problem of measuring to a surface behind a window. The fact that the reflections at the surfaces of the window have about the

same intensity as the reflected light from the CCD surface significantly affects conventional narrow band interferometry. But not an interferometer using white light. Here is the difference in path length between the reflections at the window and the signal from the CCD itself larger than the coherence length and therefore cannot affect the result.

A similar system is commercially available, providing the measurement for up to 256,000 points parallel. But the price of about 50,000 DM is to high and a special adaptation will be necessary.

## 4.2 Focus sensors

A completely different approach measuring the distance to a object with specular surface comes from geometric optics. These “focus sensors” are in daily use by most of us. Such a sensor is in every CD player and CD drive for reading the bright and dark stripes of coded data on compact discs. A lot of other applications make use of this technology. Most of these focus sensors are based on the arrangement shown in Fig. 8

There is a small light source used with no special requirements of coherence or monochromaticity. This light beam is collimated and focused by a system of lenses onto the target. From there it is reflected back the same way it is projected, entering again the optical system, collimated and using a beam splitter or grating, the reflected light is directed out of the incoming beam path. There it is then possible to analyse the way the light is reflected from the surface. The system can determine whether the target is exactly in the focus of the illumination optics and if not, in which direction and how far it is out of focus.

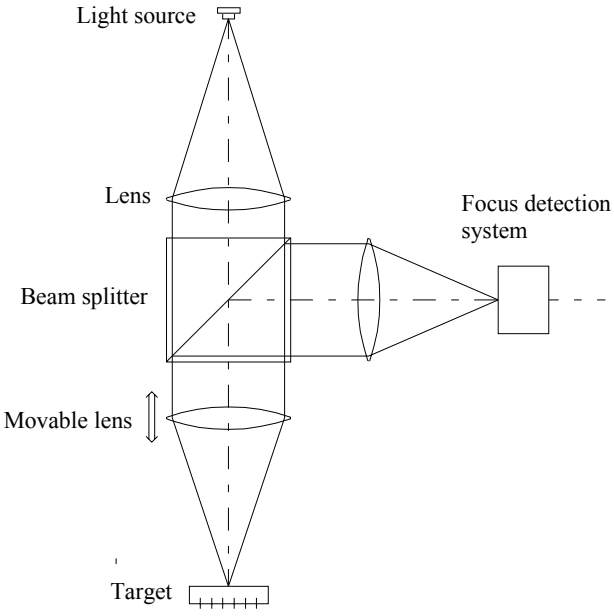


***Figure 8**. Focus distance sensor*

Since most systems for focus detection have only a small range in which they can work, it is necessary to move the whole system or only the focusing lens so that the spot is always focused onto the surface. The movement of the system or lens is to be

measured and gives the distance variation to the point at the focus position. It is possible to measure only one point at a time. As the moving mass of such a device can be very small, very fast corrections of focus are possible if the system scans over a surface.

The variety of such systems on the market is enormous, in how the focus position is detected the achievable accuracy, insensitivity for different surfaces and stand off. But none of them is fully satisfying our requirements.

## 4.3 Laser triangulation

A triangulation sensor determines the distance to an object using trigonometric characteristics. Triangulation can be done by determine two solid lines in a plane crossing at a prominent point. Triangulation sensors project a bright spot onto a surface by focusing a laser beam on it. This has two advantages: (a) There is a feature on the surface which is easy to detect. (b) The projected point can be only along the optical axis of this laser beam. So one solid line is given by this axis. A lens watches this point from beside. The lens images the spot on the surface onto a linear CCD or another position sensitive device to determine the position of the spot. Now we can determine the angle of the second solid line. Since one point of the second solid line is fixed at the center of the lens, the position of the spot is evaluated.
The rough set up of a triangulation sensor is shown in Figure 10.

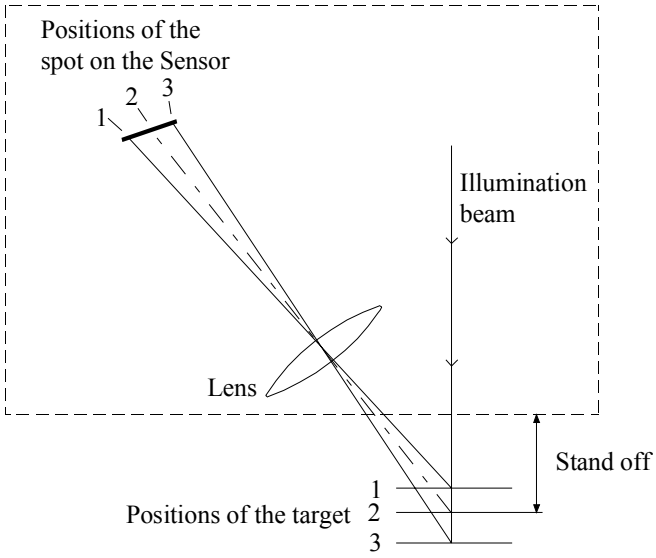


***Figure 10**. Schematic of a Triangulation Sensor. A bright spot is generated on the target by focusing a laser onto it. The spot is imaged on a linear CCD or a position sensitive diode detecting the position of it. The position of the spot on the detector is correlated with the distance of the sensor to the target.*

In practice there is no calculation done as described above. The manufacturers calibrate the sensor by moving the whole device along the axis of the projected laser beam by certain well known steps, record the corresponding spot positions and correlate them.

The accuracy of triangulation sensors depends on the working distance and measuring range. There are devices on market with a resolution of 0.2 micron and accuracy around 5 micron over the whole measurable range. The accuracy is mainly limited by roughness of the surface. This causes a speckled image on the CCD line and thereby reduces the accuracy of the spot detection (7).

Since the optics watching the spot on the surface is beside of the optical axis of the incoming beam it is only possible to detect the part of the light which is reflected diffusely. Most of the commercial available devices are calibrated and used in this way. This means that they can only be used to measure surfaces with non-specular surfaces with a high accuracy, which may cause a problem by using this for measuring backside CCDs.

The spatial distribution of the intensity of reflected light of different surfaces and under different angles is sketched in Figure 10. You can imagine the reflected light as a diagram with a clubbed shape. On a diffuse reflecting surface the reflected light is spread over broad solid angle and it is possible to see the reflection nearly from the whole space above the surface. The intensity club is broad and has about the same intensities over a wide angle. If the surface is more glossy the club of the reflected light gets more narrow. The intensity you can watch from beside decreases until zero if you have a perfect mirror.

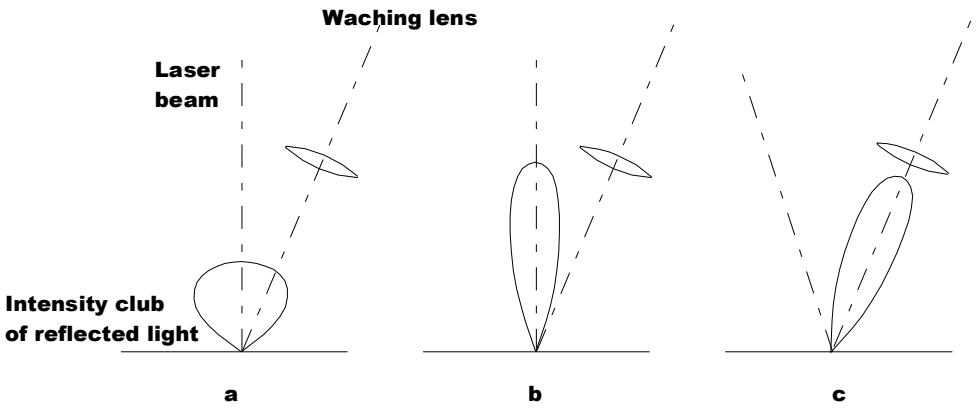


***Figure 10.*** *The intensity of the reflected light displayed as a club. The shape of the club depends on the surface. a) scattering surface. b) specular surface c) specular surface with tilted illumination*

The way out of this problem is to tilt the Triangulation Sensor by half the triangulation angle. Then the intensity club tilts too and enters again the watch lens. With this arrangement you get most of the reflected light into the watching lens and therefore the brightest possible spot on the position detector.

For special applications there are a few devices built for measuring specular surfaces but it is in general possible to use every sensor for detecting the specular reflection by tilting it by half of the triangulation angle. Since the geometric conditions of the system are changed the distance measured may not longer be correct.

Whether this technology will work for measuring the distance to a CCD must be tested. The availability on the marked is very good since such devices are widely used in industry.

### 4.4 Overview on the possible solutions.

| Technology | White light Interferometer | Triangulation | Focus sensing |
|---|---|---|---|
| Accuracy[micron] | 0.02 | 1 | 0.1 to1 |
| Complexity | High | Low | Medium |
| Effort for adaptation | High | Medium | High |
| Delivering time | 3 months | 1-4 weeks | 3 months |
| Price | 50,000 | 2000.- to 15,000.- | 30,000.- to 250,000 |

Since the price of the device does play a role and ESO does not want to spend 200,000 DM for the planarity measurement of the CCDs it will be better to do some tests with cheaper solutions to find out whether they will work too. This points clearly to triangulation sensors which are available in a broad variety. For our requirements towards accuracy only a few of them can be took into account for tests. Several companies wanted to do the tests of their systems at the companies home site.
This brings up a new problem. The fact that the CCDs which will be used in the near future are very expensive and the older CCDs have a different surface. We didn't like to hand out one of the expensive CCDs and I had to find a company (5) willing to loan us a device for testing in house. This is the easiest way to find out whether one of these devices can fulfil our tasks.

## 5. First tests with Triangulation Sensors.

TS Optoelectronic Munich was willing to loan us a Triangulation Sensor from the Keyence company for some weeks for testing. The device LC-2220 and its control unit promises under ideal conditions a resolution of 0.2 micron and a linearity error of 6 micron over the measurable range (6mm). This sensor uses a position sensitive diode for detecting the spot position. It allows setting of the gain of the current delivered by the diode and it provides an additional display for the intensity of light captured.

After putting into operation measuring a typical target, the CCD used for the FORS 2 system, it is a backside CCD from SITe with 2048 by 2048 pixels (24 micron each). It soon became clear that it is not possible to measure the surface of this CCD using this triangulation sensor when the axis of the spot projection is perpendicular to the surface, because the diffuse reflected part of the light projected onto the surface was insufficient. Hence I tilted the device by half of the triangulation angle (17.5 deg). Now the sensor got enough light for detecting the distance to the CCD.

The next step was to quantify the accuracy of the sensor. This means that I have to double check the values measured with the TS with another independently working measurement system.

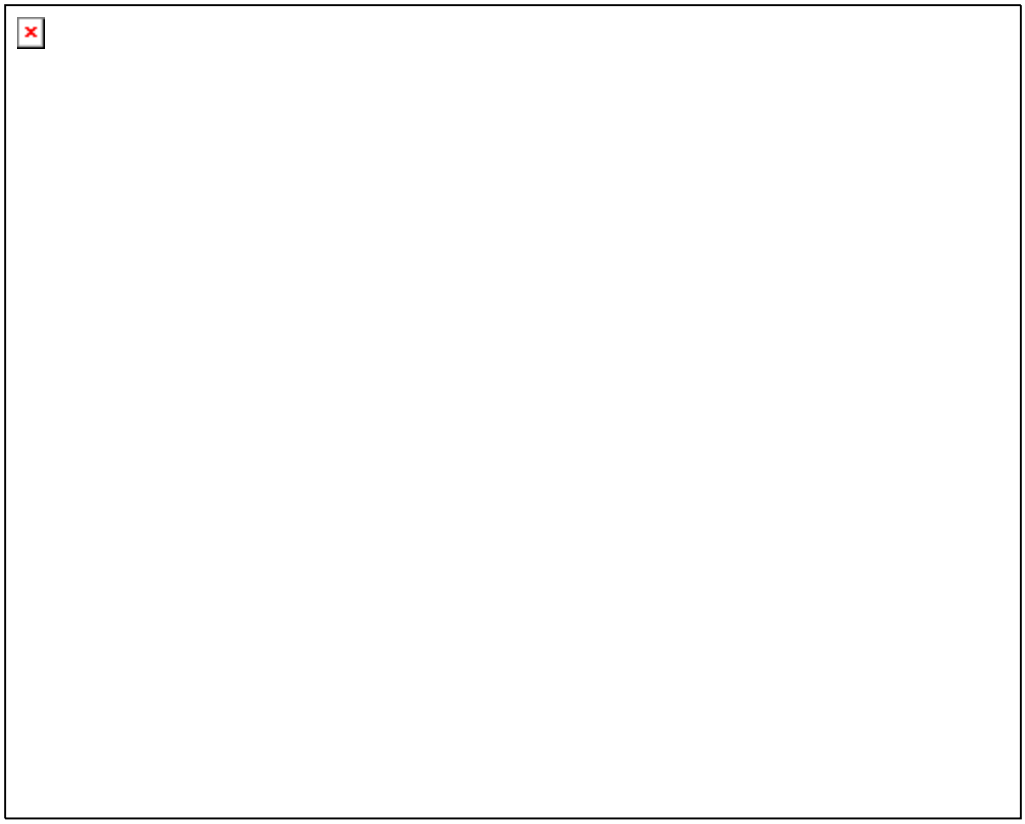

***Figure 11.*** *Test set up for the first tests done with triangulation sensors. The sensor is attached to a 3 axes translation stage which can be screwed onto a dewar. The triangulation sensor can be positioned in 3 dimension above the surface under test. For the linearity test only the upright (Z) translator was used.*

One way to do this is to mount the sensor on a linear translator with micron resolution, move the sensor with the translator by a certain distance, record the position of the linear translator and the distance of the sensor to the CCD under test. For analysis of the error the readings of the triangulation sensor were plotted in a diagram over the readings of the linear translator. Then the best fitting solid line through the numbers were calculated and subtracted from the original values measured. The remaining deviation gives a good estimation on the accuracy being achieved on this CCD and by using the triangulation sensor not in the way it is designed for. It is plotted in Figure 12.

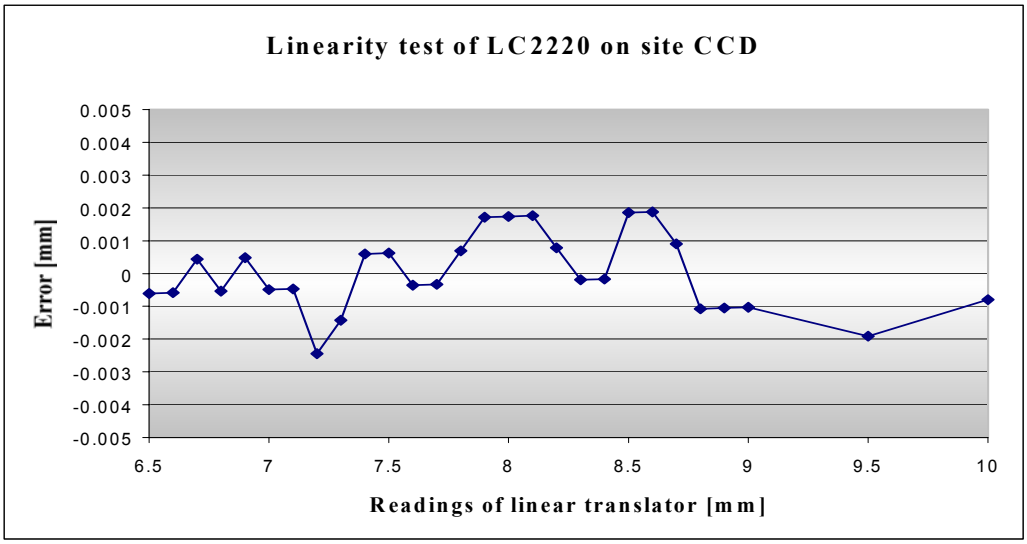


***Figure 12**. Error of the distance measurements to a SITe CCD by the triangulation sensor LC-2220 from Keyence*

To interpret Figure 12 you have to consider that the error of the linear translator is also ± 2 micron. This means it is possible that only the translator is responsible for error plotted and the sensor is more accurate. Verifying this will be quite complicated and expensive because the effort to measure a position more accurate than few microns is enormous.

The slope of the fitted solid line was 1.05 instead of 1. This means that there occurs a scaling error, probably due to the use of sensor tilted and measuring through a window. This must be examined in more detail.

In general this device seems to fulfil the requirements for accuracy and measuring range. The accuracy still can be increased averaging several measurements. It is also easy to find out whether there went anything wrong during the measurement. A completely wrong result occur for example if there gets beside the light of the main

spot from the surface light from reflections at the protection window on the detector. The signal then no longer corresponds with the distance to the CCD. In the diagrams showing the error this shows as a kink of the plotted values. To prevent this error I blocked the reflections by a additional stop in front of the watching optics in such a way that only the light coming from the desired surface is able to reach the position sensitive diode. This shrinks the measurable range of the Sensor to about 4.5mm.

The results in Fig. 14 were achieved on one special CCD type. The next step is to verify whether this is repeatable on the other CCDs in house. There was just a mosaic to be assembled for ESO's UV-Visual Echelle Spectrograph (UVES) consisting of one EEV CCD and one MIT/LL CCD with enhanced coating. This is an ideal test piece since it is possible to test different CCDs with exactly the same setup. The only change done is to move the sensor on the X-Y-Z stage from one position to another. Repeating the measurement above with fewer points uncovered the same behaviour on the surface of the EEV CCD shown in Fig.13.

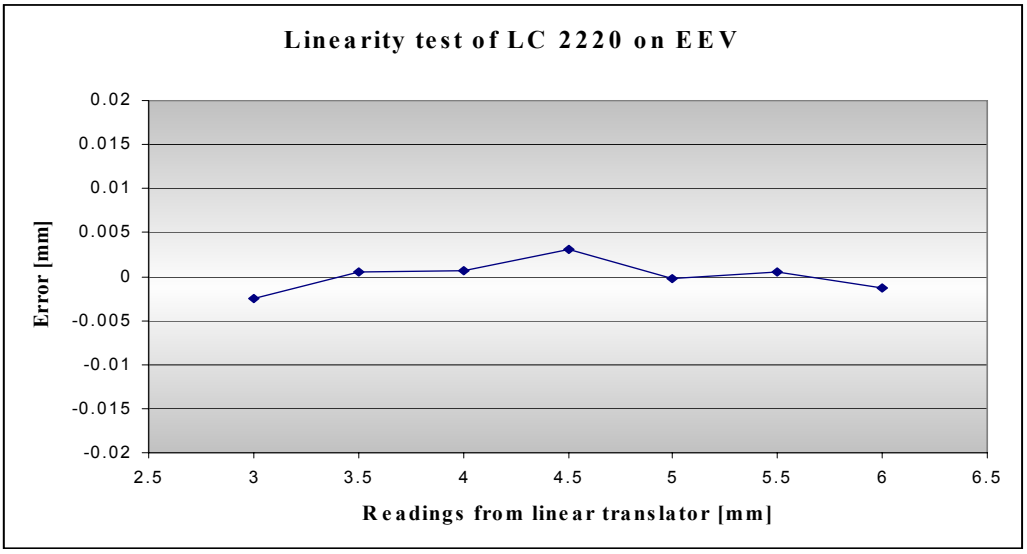


***Figure 13**. Error of the distance measurements on EEV CCD by the triangulation sensor LC-2220 from Keyence*

The slope of the best fit line was again 1.05. Indeed the range of which it was possible to get a linear behaviour of the measurement was reduced to 3 mm and the error is bigger, but still close to the requirements.

The result on the MIT/LL CCD was quite strange. The remaining error is plotted in Figure 14

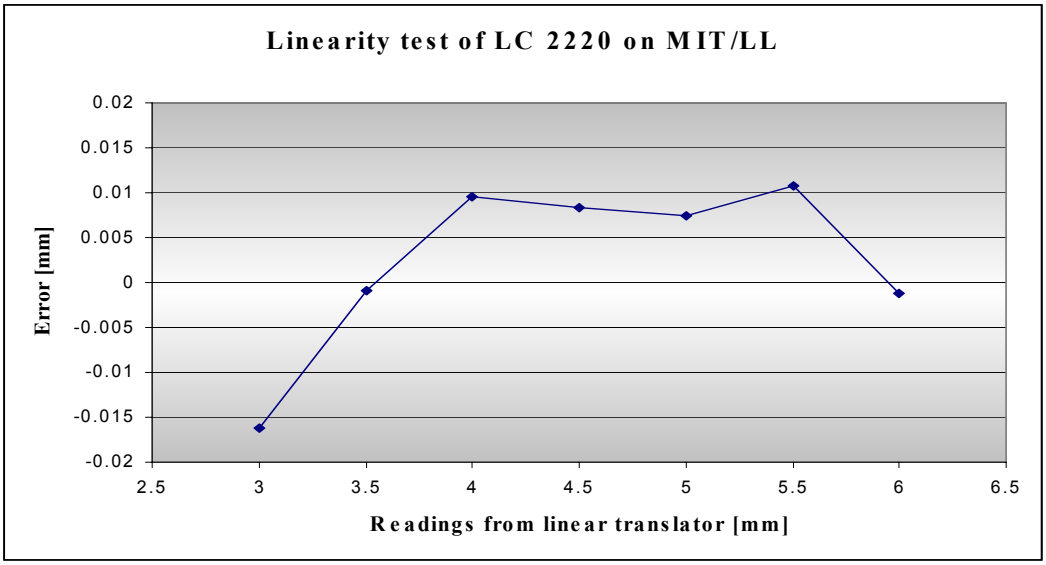


***Figure 14.*** *Error of the distance measurements to a CCD of the Triangulation Sensor LC2220 from Keyence*

One difference is that the remaining deviation of the measured points to the fitted line is much larger, if the same range is evaluated as in the test on the EEV CCD. Another difference is the change of the slope of the fitted line to 1.008. It is difficult to understand how it should be possible that under exactly the same geometric conditions the sensor measures with different scales on different surfaces.

I made further measurements of the two CCDs assembled in the UVES mosaic for quantifying the surface of these CCDs. Therefore the co-ordinates of a few points spread equally on the surfaces were recorded and analysed with Matlab [Appendix B]. With the measured points a best fit plane was calculated, the plane was then subtracted from the original measurements. The remaining deviation of the points measured is plotted in the graphs in Figure 15 and Figure 16. The surface plots were generated by using the Matlab command “SURF” which uses a spline algorithm. The circles mark the points measured.

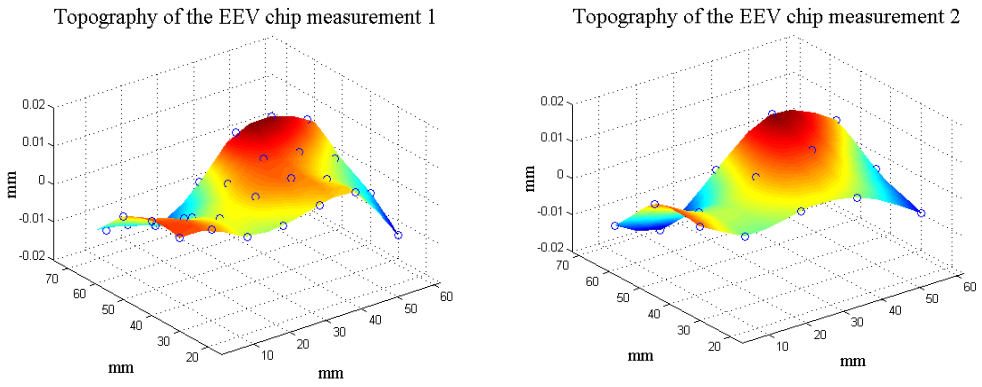


***Figure 15.*** *Deviation of the surface of a mechanical sample from EEV from a flat plane. Left measured close to the zero point of the Triangulation Sensor LC2220 (RMS 5µm, PV 23µm), right with an offset of 1.5 mm (RMS 6µm, PV 22µm).*

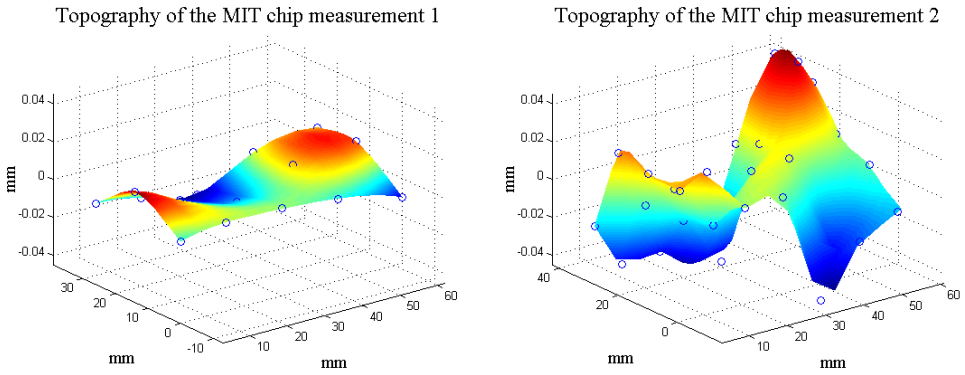


***Figure 16****. Deviation of the surface of CCD MIT/Lincoln Lab CCD from a flat plane. Left measured close to the zero point of the Triangulation Sensor LC2220(RMS 6µm, PV 25µm), right with an offset of 1.5 mm(RMS 28µm, PV 105µm)*

In Figure 15 both sets of measurements give about the same shape of the surface of the EEV CCD and this independently from the offset of the sensor. Doing the same on the anti reflection coated CCD from MIT/LL shows for both measurements quite different topographies of the same object (Figure 16.). Despite the fact that the measurements seems to be more noisy the topography shows 4 times higher structures if the CCD is measured with a larger distance of the sensor to the CCD.
Something seems to be really wrong.

I mentioned already that the device can also display the intensity collected by the position sensitive diode. Comparing the brightness values of the EEV and MIT CCDs

revealed a difference of a factor up to 100 which the MIT CCD reflects less light than the EEV CCD. For the measurements on the MIT CCD the highest possible gain was used and the signal from this CCD was nearly too dim to be detected well. For measuring dim surfaces the Keyence LC2220 sensor has one main disadvantage, it is not able to regulate the laser power. Probably the different behaviour depending on the intensity has to do with a poor linearity of the position sensitive diode at low intensities.

I have shown that a triangulation system will work for measuring such a CCD, only the power of the laser or the sensitivity of the detector seems to be the problem. Realising this I started looking for a company willing to loan us a device with a regulation of the laser power to the brightness of the spot on the detector and/or another detector for the spot position.

There are two other companies providing triangulation Sensors with a linear CCD as detector and a power regulation. I repeated the previous linearity test with a triangulation sensor from Technigues de Pointe SA (Winterthur Switzerland) with the result that this device suffers from bad linearity, which has mainly to do with the use in the direct reflection mode for which it is not linearised. The device from the second company Micro Epsilon showed better results. The deviation of the distance measured with this triangulation sensor was again compared with the movement of the linear stage and the remaining error is shown in Figure 17.

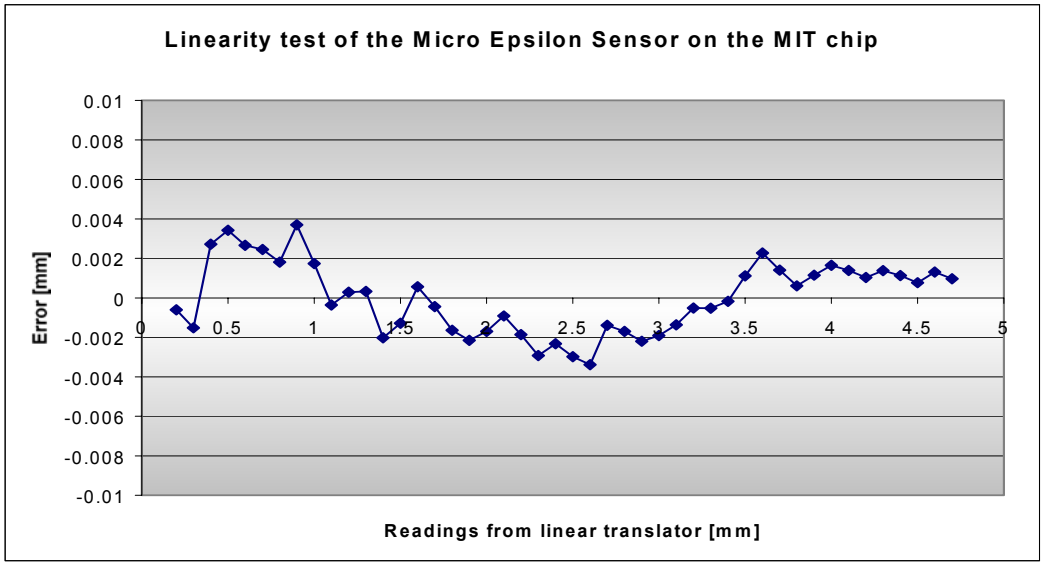


***Figure 17****. Error of the distance measurements to a MIT CCD by the Triangulation Sensor ILD2000-5 from Micro Epsilon. The bow of the points in the diagram is repeatable and can be removed numerically.*

The error curve shows a systematic bow within ± 3 micron to which noise is added. Since the shape of the curve is repeatable on different surfaces and at different positions on the linear translator used, the source of this deviation may be inside of the sensor. In this case it is possible to remove this bow numerically. This means that it is not sufficient to calculate the deviation by subtracting the best fit line. Rather we have to fit a polynomial with a higher degree for linearising this curve. The slope of the best fit lines through the measurements on different CCDs are the same. I have checked this by measuring the linearity on the front side of a window, on a CCD from EEV with a coating optimised for green wavelengths and on a MIT/LL CCD with a coating optimised for red and near infrared light. Especially the MIT/LL CCD caused the problems of the Keyence triangulation sensor.

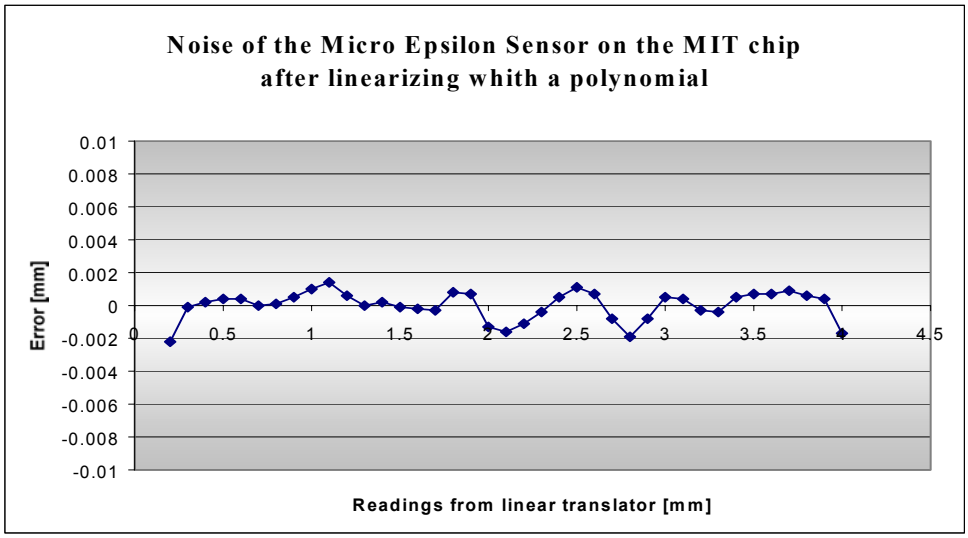


***Figure18**. The error of the distance measurements to a MIT CCD by the Triangulation Sensor ILD2000-5 from Micro Epsilon. The measurement was linearised by using a polynomial of the following kind: $y=a_0 + a_1*x + a_2*x^2$ The bow of the points in the diagram is repeatable and can be removed numerically.*

Figure 18 shows the remaining error after the measurements have been linearised by a polynomial of the form $y=a_0 + a_1*x + a_2*x^2$. The remaining error has a standard deviation of 0.9 micron. Don't forger the error may be introduced by the linear translator.

## 5.1 Flatness measurements at ESO's Wide Field Imager (WFI)

With the experiments above I have shown that this triangulation sensor is in general qualified for measuring the flatness of CCDs of different kinds. Since there was a big mosaic camera with 8192 by 8192 pixels consistingof 8 CCDs (2048 by

4096 pixels each) to be assembled when I had found this possibility for measuring CCDs it is clear that this technology was used for the flatness measurement of the CCDs in this instrument. To do this we needed a means to position the sensor above the mosaic and to measure the co-ordinates of the sensor. After a modification of a 3D measuring machine present at the metrology lab of ESO we were able to do this.

***Figure 19**. Set up for the provisional measurement of the planarity of the CCDs of WFI. The co ordinate measuring machine (back ground) is used for positioning the Triangulation sensor attached to the movable arm of the measuring machine over the camera head. The data is than entered by hand to the laptop on which screen a preliminary surface analysis is displayed.*

In Figure 19 the co-ordinate measure machine is shown. The triangulation Sensor is attached to the movable arm of the measure machine. Now it is possible to move the sensor only in the X-Y plane (parallel to the table) and measure its co-ordinates. The

triangulation sensor measures its distance from the CCD below. By positioning the sensor at different points in a regular grid above the CCD mosaic and recording the position of the sensor and its distance from the CCD we are able to reconstruct and analyse the topography of the detector surface. Doing this was time consuming. Since all the data has to be entered into a laptop manually.

Afterwards the data was analysed by using Matlab. For a more convenient analysis some functions were written which are described in Appendix B. For analysis the best fit plane through the points measured was determined and subtracted from the original points and for the remaining error the RMS value and the distance from peak to valley was calculated. This gives you a measurement for the flatness of the detector surface.

Additionally several points at the flange where the whole camera will be attached to the telescope were recorded and analysed in the same way. The difference of the slope of the planes through both sets of measurements gives a value of the tilt of the detector surface towards the flange, which is used as a reference. This value is useful for the alignment of the mosaic inside of the cryostat or of the whole instrument at the telescope.

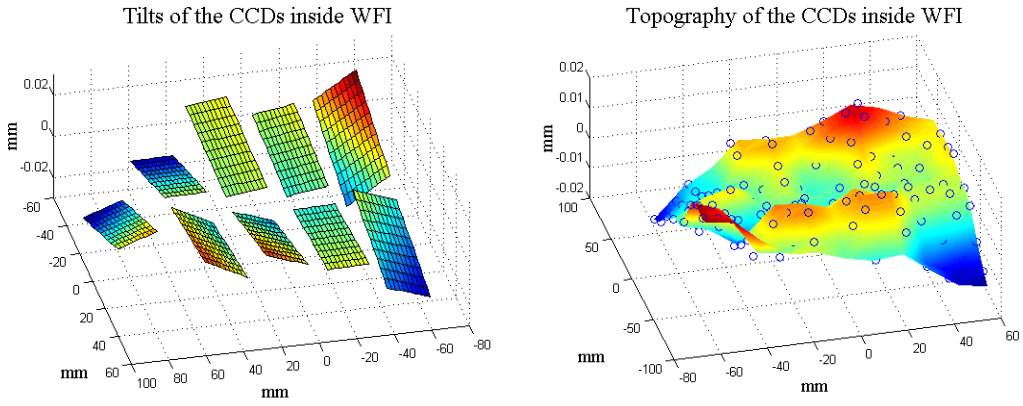


***Figure20 a,b**: Left: The Best fit planes for each of the CCDs inside of the WFI are plotted. The CCDs are assembled in two rows of 4 CCDs each. The single CCD at the left is used for tracking the telescope. Right: The surface of all the CCDs is molten together and displayed with the SURF command from Matlab which uses a spline approximation.*

For the example above the measured values are deviated around the best fit plane with a RMS value of 6.6 micron and the peak to valley distance of the worst points is 37 micron. The surface of all CCD together was tilted relative to the flange in X direction of 0.1 mrad and in Y direction by 0.6 mrad. The error of the flatness was

well inside the specs of 50 micron and the tilt of the detector surface relative to the flange was corrected when the camera was attached to the telescope.

It is still very time consuming to position the sensor manually, entering the data into the computer by hand and analysing it afterwards single steps. There are also several possibilities where the final result loses reliability just by introducing typing errors.

It is important to have this procedure of measuring and analysing the flatness automated for increasing the reliability of the result and saving manpower

Also the needed accuracy of a single point measured must be determined. Of course if the single measurement has a certain error the error of the fit plane through a cloud of points measured will be smaller, but the correspondence between the number of points measured, its accuracy and the remaining error of the best fit plane must be examined.

Another point fully neglected up to now, is the influence of the window on the result of the measurement.
So I can derive several tasks to be done:

Conception and Design of the Measuring machine
Looking for a X Y stage
Examining the influence of the window between the CCD and the sensor
Examining the error propagation for the mathematics used
Software for automated measurement and analysis

# 6. Influences on the measurement by laser triangulation sensors

## 6.1 Influence of the tilt of the triangulation sensor

A triangulation sensor measures the distance to the surface by using an internal co-ordinate system. The orientation of this co-ordinate system is fixed by the axis of the laser beam used for the projection of a spot onto a surface. The triangulation sensor we are using is designed for the case that the axis of the illumination beam is perpendicular to the surface, so it measures the distance of the spot from a reference plane at the sensor along the axis of the laser beam.

Since the triangulation sensor does not know anything about the angle it has to the surface it still displays a distance of the watched spot to the reference along the axis of the laser beam. This corresponds no longer with the real distance of the surface to the sensor in the rotated co-ordinate system.
Figure 21 shows a sketch of the geometrical conditions for the sensor used tilted.

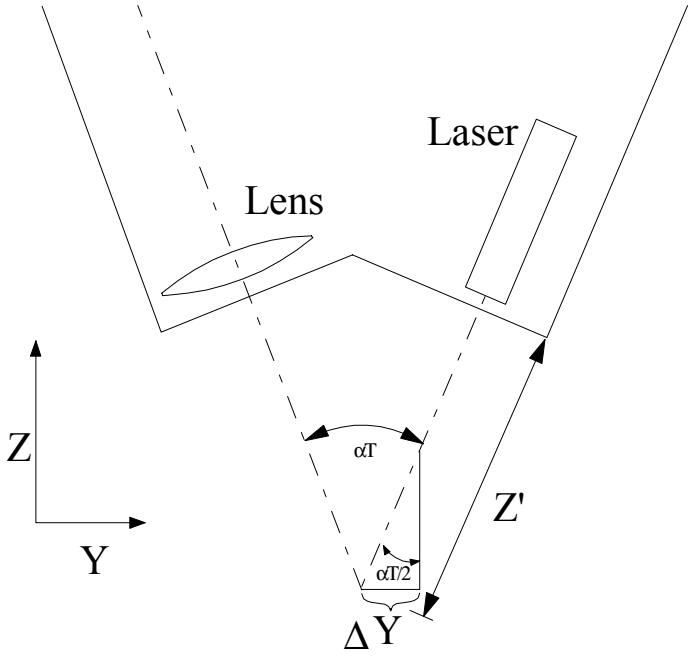


***Figure 21.*** *Triangulation sensor if it is tilted by half of the triangulation angle. The sensor measures the position of the spot along the axis of the incoming beam and displays a signal proportional to this position. If this axis is tilted the measured distances must be transformed to the co-ordinate system of the measuring machine.*

The triangulation sensor watches a point moving along the line of the illuminating laser beam (z') and delivers a signal proportional to the position of the spot along this line. Now the co-ordinate system of the sensor is tilted and must be transformed into the co-ordinate system of the measuring machine.
The distance measured can be corrected by using the following formula.

$$Z = \frac{Z'}{\cos\left(\frac{\alpha T}{2}\right)} \qquad [1]$$

Where Z is the corrected value, Z' is the sensor reading and αT is the angle of the tilt of the illuminating beam. This will be half of the triangulation angle if the sensor is used for measuring specular reflections.

The correction factor

$$\frac{1}{\cos\left(\frac{\alpha T}{2}\right)}$$

was already experimentally found. It is the slope of the best fit line determined during the linearity test done for qualifying the sensor. The experiments gave 1.05 for the Keyence device with a triangulation angle of 36 deg. The correction factor calculated is 1.051. for the Micro epsilon device it was measured to 1.063±0.005 and is calculated to 1.0615. So it is well inside of the confidential interval for this size.

Another error occurs on the position of the measured point. If you move the sensor to a certain point in X and Y direction and if the distance to the surface varies much the point to which the sensor is positioned does not correspond with the position it measures. It deviates in Y direction. This may introduce a systematic error in Z if a surface is bend strong and must thereby corrected by.

$$\Delta Y = \Delta Z' * \sin(\tfrac{\alpha T}{2}) \qquad [2]$$

ΔY is the correction of the Y co-ordinate and as ΔZ' the Sensor reading can be used. The correction of the sensor position can be done in two ways:

a) The co-ordinates of the point measured can be corrected.
b) The position of the sensor can be corrected so that the laser spot hits the surface at the same position independent of the distance to the surface it has. This can be don on line using the current distance read from the sensor.

## 6.2 Influence of the window between the CCD and the sensor

For most measurements of the flatness of a CCD or a mosaic of them, a window for protection will be between the triangulation sensor and the CCD. Therefore the influences of this window are of significant interest. The beam will get refracted there which may cause a wrong or shifted result. The size of this deviations and the sensitivity of the device for tilts of the window and CCD I will examine now.

### 6.2.1 Measuring the distance to the backside of a optical flat

A simple example for a deviation of the measured value and its real dimension is the measurement of the distance to the backside of a glass plate. The window is thought to be a perfect optical flat and perpendicular to the symmetry axis of the triangulation sensor, which is tilted by half of the triangulation angle. A detailed view of the ray path gives Figure 22.

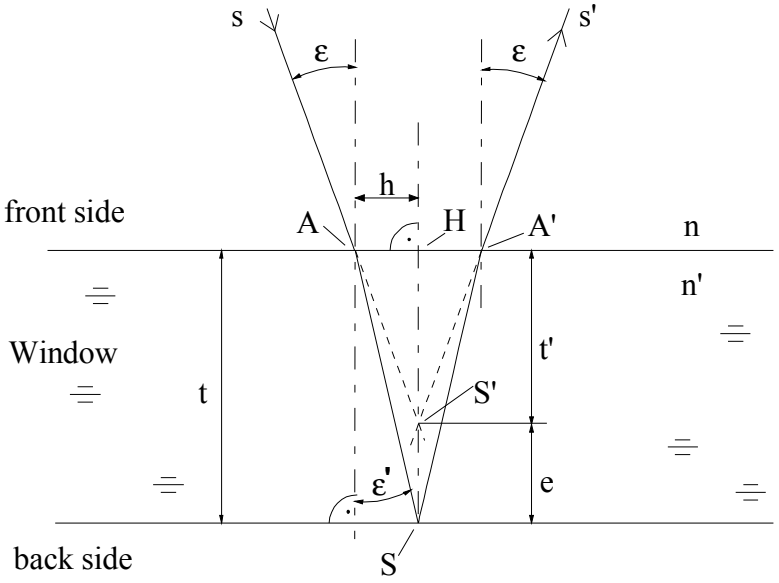


***Figure 22**. Sketch of the beam path for a measurement of the distance to the back side of an optical flat by a triangulation sensor.*

The incoming light beam with angle ε is refracted at the front surface of the window (point *A*), reflected on the backside (point *S* ) and exits the window again at the front side (point *A'*). What the sensor sees is the beam coming from the Point *A'* with the angle ε. Since the triangulation sensor expects to see a spot along the axis of the incoming beam we have to lengthen the axis of the original illumination beam and the beam after it got reflected and refracted in the directions they have outside the window. The crossing of both lines defines the position at which the triangulation sensor will see the spot. The distance to this point is the distance the triangulation sensor will measure.

For the calculations I will take the front surface of the optical flat as a reference, since the distance to there can be measured with the sensor without the disturbing influence of the window. t indicates the real distance between the front and back side (thickness) of the optical flat t' the one measured by the triangulation sensor.
Now we are interested in getting the real distance to the backside of the window or the deviation between the real distance of the sensor from the window and the displayed one, titled *e* . It can then be calculated by.

$$e = t - t' \qquad [3]$$

Using an auxiliary size *h* it applies for the triangle SAH

$$h = t * \tan \varepsilon'$$

And for the triangle S'AH

$$h = t' * \tan\varepsilon$$

From those equations follows

$$\frac{t}{t'} = \frac{\tan\varepsilon}{\tan\varepsilon'} = \frac{\sin\varepsilon * \cos\varepsilon'}{\cos\varepsilon * \sin\varepsilon'}$$

with

$$\sin\varepsilon' = \frac{n}{n'}\sin\varepsilon \quad \text{and} \quad \cos\varepsilon' = \sqrt{\left(\frac{n'}{n}\right)^2 - \sin^2\varepsilon}$$

We can write for the true thickness of the window

$$t = t' \frac{\sqrt{\left(\frac{n'}{n}\right)^2 - \sin^2\varepsilon}}{\cos\varepsilon} \qquad [4]$$

and the error e for n=1 is

$$e = t\left(1 - \frac{\cos\varepsilon}{\sqrt{\left(\frac{n'}{n}\right)^2 - \sin^2\varepsilon}}\right) \qquad [5]$$

The deviation of the measured distance is influenced by the thickness of the optical flat and its index of refraction, if we take the angle ε as fixed.

This formula is also useful for the case that behind the window is vacuum. In this case for n'=1, and for n the index of refractivity of air must be taken. The additional error can be added to the error of the other influences calculated, since the change of the refractive angle due to this effect is small. This error depends on the distance between window and CCD. For example a window 10 mm above the CCD causes with a ε=19.6 deg. and n=1.003 a error of 3 micron.

## 6.2.2 Measuring on a glossy surface through a window:

To measure distances to a CCD through an optical flat will be the most common case. Doing this the distance measured by the triangulation sensor will be again influenced by this optical flat. In this case the geometric conditions get more complicated.

The beam path through the optical flat to a specular surface and back to the triangulation sensor is outlined in Figure 23.

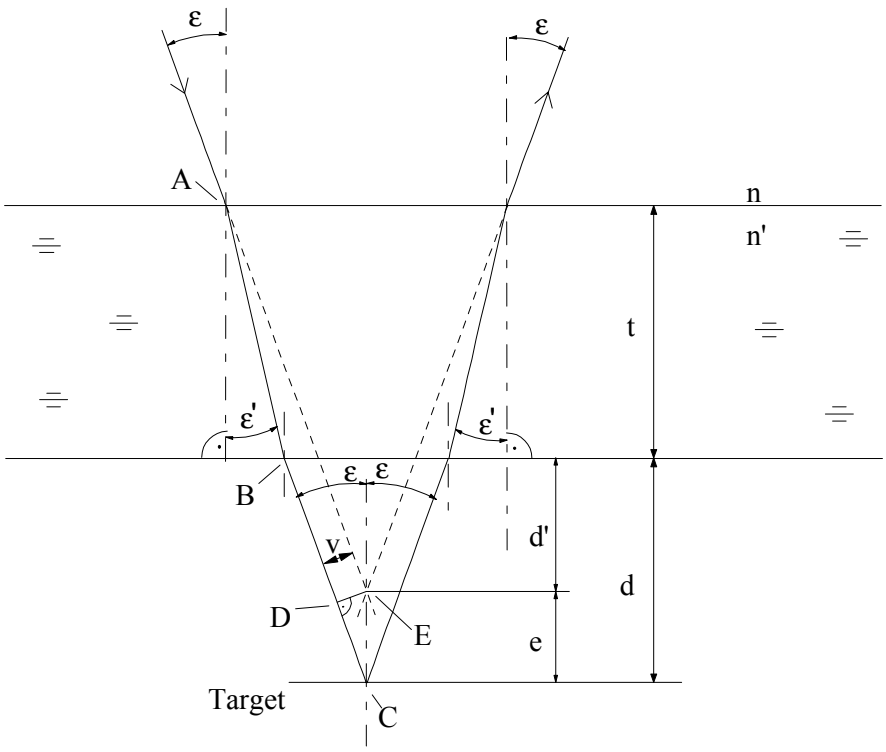


***Figure 23**. Sketch of the beam path of the measurement with a triangulation sensor of the distance to a specular surface behind an optical flat.*

The optical flat with the thickness t, refractive index n' has a distance to the target of d. The laser beam enters the window at point A, gets there refracted and propagates through the glass with ε' to the point B where it gets refracted again exiting the optical flat. The beam is after its passage of the optical flat parallel to the incoming one. It gets only an offset v (See appendix A), then it hits the surface at point C. Since all surfaces are perpendicular to the symmetry axis of the triangulation sensor the path of the illumination beam back to the watching optics is symmetric to the incoming one. Extending the beams in the direction they have above the window gives the point where the Triangulation sensor sees the spot. We calculate now the distance *e* of the spot seen by the sensor to the position it hits really
For the triangle D E C we can write

$$\sin \varepsilon = \frac{v}{e} \qquad [6]$$

with

$$v = t \sin \varepsilon \left( 1 - \frac{\cos \varepsilon}{\sqrt{n'^2 - \sin^2 \varepsilon}} \right) \qquad [7]$$

From appendix A we can write for the error

$$e = t \left( 1 - \frac{\cos \varepsilon}{\sqrt{n'^2 - \sin^2 \varepsilon}} \right) \qquad [8]$$

Note that this deviation depends only on the index of refractivity and the thickness of the glass. The distance between optical flat and CCD plays no role.

If you are not interested in getting the real distance between the CCD and the optical flat and you are only interested in the topography of the CCDs which means a measurement relative to a imaginary plane, this correction can be neglected. It is only of importance if you want to know real distances from the triangulation sensor to CCDs.

The parallelism of the target and the optical flat we assumed for the calculations above will not be true in practice. It is the task of the measuring machine to measure this tilts.

### 6.2.3 Influence of tilted surfaces to the measurement.

In the most common case the CCD and window may be tilted differently with a different amount and orientation of the tilt. Due to surface imperfections of the CCD a tilt will remain, even if the chip itself is as well aligned as possible. For example consider a domed CCD. Only one point of its surface can be parallel to the window in front. For all other points there will be a relative tilt between them which may influence the measurement. Therefore it is important to know the influence of this tilt on the measurement.

For the following considerations it is better to describe the tilt of a surface by its shares in x and y direction than by amount and orientation.
Doing this we get tilts of 2 bodies in two directions. A total of 4 affecting factors. Since the tilts in x and y direction have different influences on the measurement we have to discuss them separately. First I will calculate the influence of Y-tilts on the measurement ( See Fig.30 ). The calculation is the same as we have done above, we look at which position the triangulation sensor sees the spot. Then we calculate the vertical offset of this point to the point on the CCD where the light is reflected.

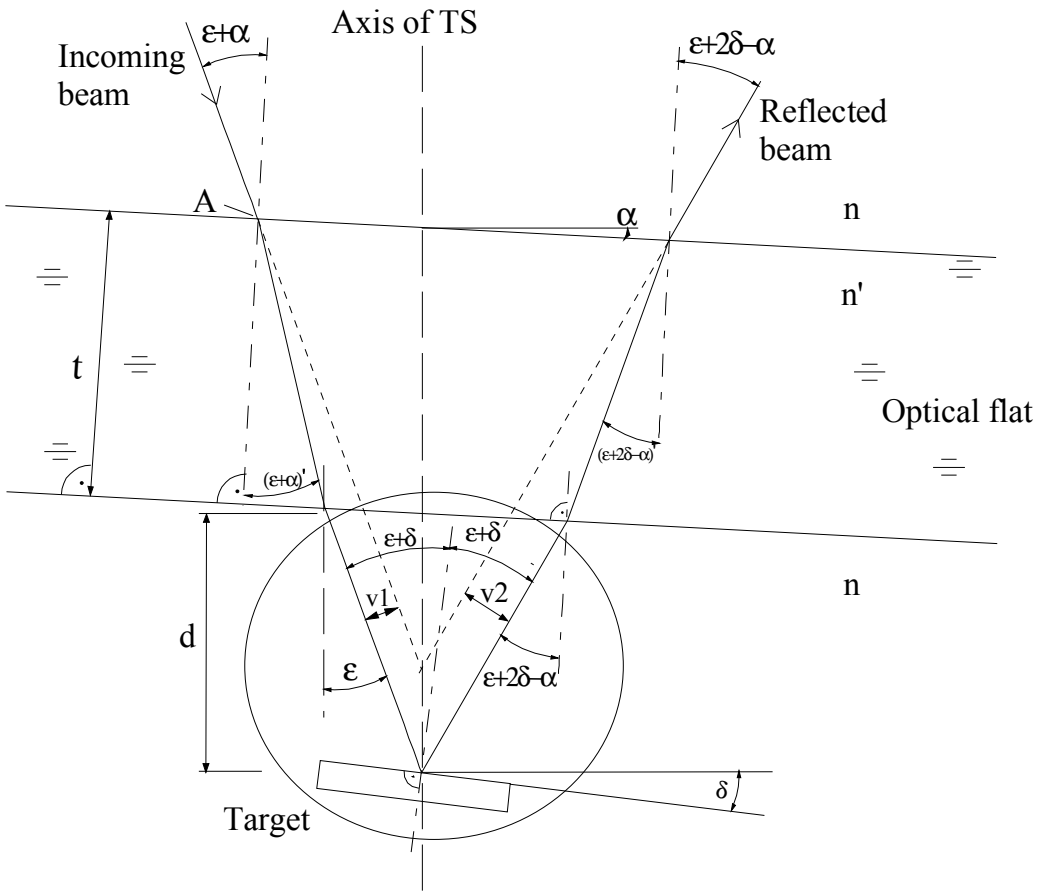


***Figure 24.*** *Sketch of the beam path for the measurement to a specular surface behind an optical flat. In this case window and target may be tilted against the axis of the triangulation sensor.*

There is one big difference to the calculations without tilted surfaces, now we do not have a symmetry in the path of the beam to the CCD and the path from the CCD to the sensor. The incoming beam gets an offset v1 until it is reflected at the tilted surface. Then it gets reflected with the result that the reflected beam gets a different incidence angle to the window than the incoming one and thereby a different offset v2. Extending the beams from above the optical flat back again gives the point where the sensor will see the spot. For the calculation of the error e in this case Figure 24 shows more details of the geometric conditions.

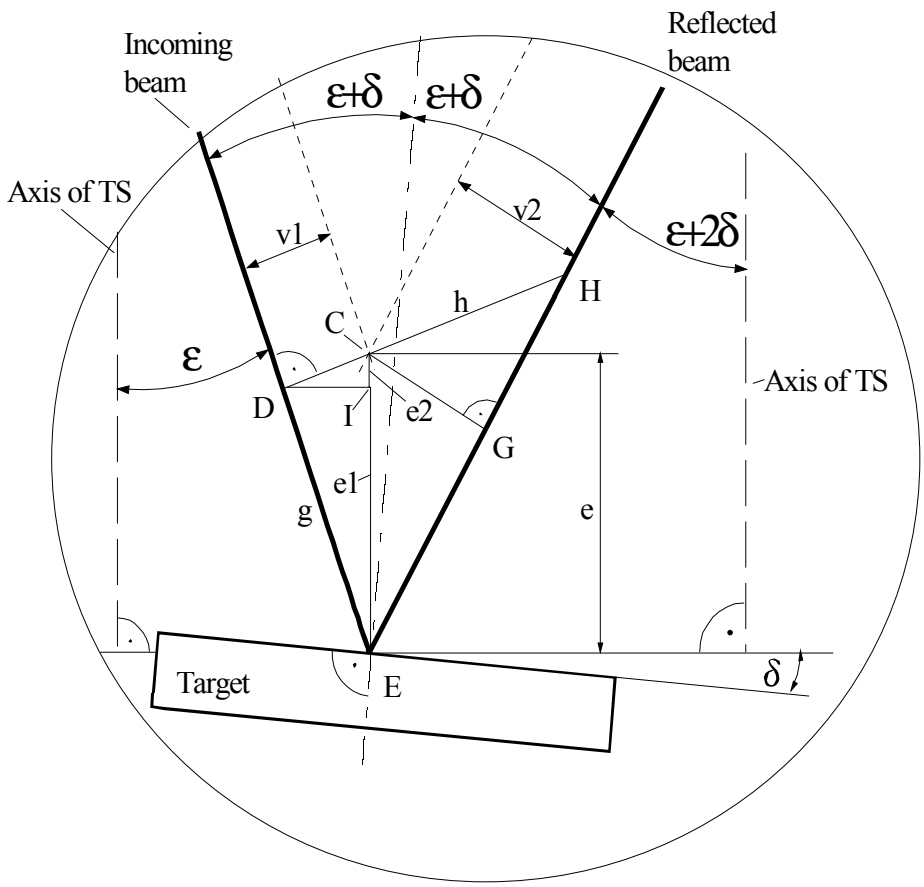


***Figure 25**. Detailed view to the beam path near the CCD of Figure 24.*

We know the following sizes: the angle of the beam before it is reflected $\varepsilon$, the thickness of the window *t* and the index of refractivity of its material *n'*. Using this we can calculate the parallel offset *v1* of the incoming beam. The tilt of the optical flat ($\alpha$) relative to the symmetry line of the triangulation sensor we can measure. Further we assume that we know the tilt of the CCD to the symmetry line $\delta$ .This gives us the inclination of the reflected beam towards the symmetry axis of the triangulation sensor as $\varepsilon+2\delta$ and as $\varepsilon+2\delta-\alpha$ towards the window. Now the offset of the reflected beam *v2* can be calculated.

For a calculation of the error e we have to split the task into smaller steps.
The error e we split into

$$e = e1 + e2 \qquad [9]$$

e2 we can calculate directly from the triangle C D I

$$e2 = v1 * \sin(\varepsilon) \qquad [10]$$

Using the triangles H C G we can write for the length h

$$h = \frac{v2}{\cos(2*(\varepsilon+\delta))} \qquad [11]$$

g we can describe by using D E H as

$$g = \frac{h+v1}{\tan(2*(\varepsilon+\delta))}$$

And get

$$g = \frac{v2+v1*\cos(2*(\varepsilon+\delta))}{\sin(2*(\varepsilon+\delta))} \qquad [12]$$

Final e1 is

$$e1 = g*\sin(\varepsilon) \qquad [13]$$

With v1 as

$$v1 = t*\sin(\varepsilon+\alpha)\left(1-\frac{\cos(\varepsilon+\alpha)}{\sqrt{(n')^2-\sin^2(\varepsilon+\alpha)}}\right)$$

And v2 as

$$v2 = t*\sin(\varepsilon+2*\delta-\alpha)\left(1-\frac{\cos(\varepsilon+2*\delta-\alpha)}{\sqrt{(n')^2-\sin^2(\varepsilon+2*\delta-\alpha)}}\right)$$

The error e can be determined.

Since the angles inside of the expressions are different a simplification of the set of formulas to a small and easy applicable formula seems not to be possible. And only putting the expressions above together to a very big one does also not help much in making it more descriptive.

The distance of the optical flat to the CCD is not contained in any of the formulas above needed for calculation of e. So the assumption that the tilt of the CCD is known is correct since we can first measure the surface, determine the tilts and correct the offsets later, if necessary.

To get a feeling for the size of the additional error due to tilted surfaces the error is plotted as a function of the tilt. As the amount of the error due to the tilt is small I subtracted the offset of the non tilted case from the error taking tilt into account.

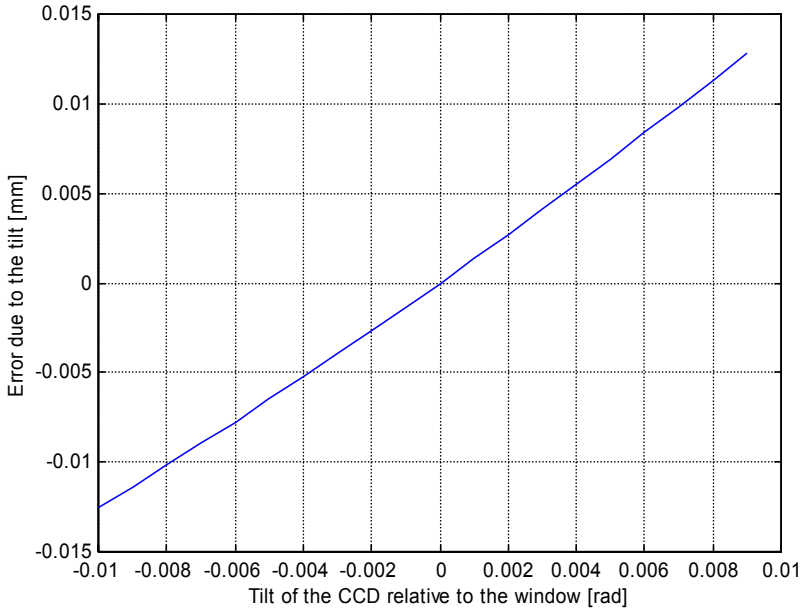


***Figure 26**. Deviation of the distance measured to a CCD by a triangulation sensor as a function of the relative tilt of the CCD to the symmetry axis of the triangulation sensor.*

The simulation was done for an optical flat with a thickness of 10mm an index of refractivity of 1.5. Only a tilt of the CCD was taken into account. A rough estimation for the size of this error and this window is about 1.2*tilt of the CCD in rad.

The second influencing factor, the tilt of the optical flat while the CCD stays perpendicular to the axis of the triangulation sensor, is plotted for the same window and tilts in Figure 27.

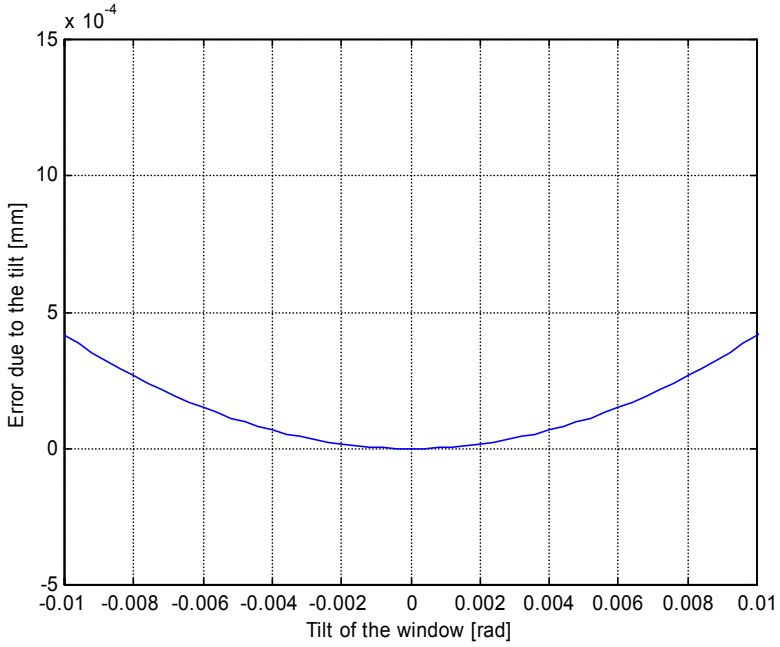


***Figure 27.*** *Deviation of the distance measured to a CCD by a triangulation sensor as a function of the tilt of the optical flat in front of the CCD, relative to the symmetry axis of the triangulation sensor.*

Note the different scale applied to this graph. Because of the vanishing size of the influence we can neglect it for further considerations and discuss the influence of tilted CCDs.

If every CCD assembled in a mosaic is tilted differently we can measure their tilts but the steps between them will contain a systematic deviation. As an example the biggest difference in the tilts of all CCDs inside the WFI mosaic were 0.002 rad. Applying the formulas above we get a systematic error of 2.5 micron for the offset between different CCDs due to their tilt.

Another case of interest is, what happens if the surface of a CCD is bent so strongly that the tilt of the surface varies significant. The topography of the CCD will be wrong. Typical topographies for the most common CCDs form EEV varies between ±10 microns. If we assume that the surface does not vary between both values on a scale smaller than 10 mm we get a tilt of 0.002 rad. This tilt generates an error of the topography of ±2.5 microns (10mm glass, n=1.5). This is also in a region allowing to neglect it as long as the topography is not of big interest.

Discussion of tilts in X direction.

Up to now we considered only tilts in Y direction (see Figure 33.). The spot gets shifted along the linear CCD inside the triangulation sensor due to a Y-tilt. For a tilt in X direction the spot will get a displacement, perpendicular to the displacement resulting from the Y tilt. This means that the spot gets a displacement crosswise to the CCD line so that the spot may not hit the CCD line. For this kind of displacement the formulas above can be applied and give for the same optical flat and for tilts up to 0.01 rad an error of the spot position of below 1 micron. This spot is mapped from the optics onto the CCD line with a magnification of two. So the transversal displacement on the CCD line will be below 2 micron. This will have no big influence, since the size of the spot projected on the CCD line has a size of 200 micron.

# 7. Influence of the error of single points to the error of the alignment of a CCD.

Every measurement contains an error. Also every value used for the alignment of the CCD. These errors propagate through the mathematics used up to a remaining uncertainty of the correction. It must not limit the quality of the alignment and therefore be far smaller than the tolerance. A guideline for the necessary fidelity of an instrument is that it should be 7 to 10 times more accurate than the tolerance measured. Applying this rule to the tolerances given from the highest requirements to the planarity of a single chip of 20 micron and of a mosaic of 50 microns gives tolerances for the measurement between 2 and 7 micron.

This is valid for the corrections to be applied to the CCD's. Since we do not measure a surface at once and the CCD itself isn't flat we can not take these values as the requirements to the single measurement.

To get the values for correction of a chip, two planes are to be measured, one used as the reference to which the chip should be aligned and the chip itself. The best fit plane is calculated for both sets of values. To be able to correct the chip the differences between both planes at the supporting points of the chip then must be calculated. The remaining error of these corrections should then be smaller than the tolerances for the alignment of the detector. To describe the allowed deviation of a single point measured as a function of the allowed error of the correction I simulate an initial uncertainty and calculate its propagation up to the final result.

The first step coming from two clouds of points in space and going to the final correction is the determination of the parameters of the best fit plane. For the fit I used the following formulation for the plane:

$$z = a_0 + a_1 x + a_2 y \qquad [14]$$

The vector of the parameters $\underline{a}$ is then determined by minimising the mean squared difference of the points measured to this plane

$$\underline{z} = H * \underline{a} + \underline{e} \qquad [15]$$

and resolving this expression for the Gauss Markoff Estimator $\underline{\hat{a}}$

$$\underline{\hat{a}} = (H^T * H)^{-1} H^T * \underline{z} \qquad [16]$$

$\underline{z}$ is a vector containing the measured values, $\underline{e}$ contains the difference between the estimated plane and the measurements and $H$ the formulation for the plane containing the positions of the values in $\underline{z}$. For our special case it is shown below.

$$H = \begin{Bmatrix} 1 & x_1 & y_1 \\ \vdots & \vdots & \vdots \\ 1 & x_i & y_i \end{Bmatrix}$$

The error of these parameters can be determined after introducing the covariance matrix R defined as

$$R = E\left\{\underline{e} * \underline{e}^T\right\} \qquad [17]$$

Since the errors of each value measured are equal we can simplify this expression to

$$R = \sigma_z^2 * [I]$$

Here is $\sigma_z$ the standard deviation of the measurement.
The usage of this simplification in the following expression

$$E\left\{\underline{\hat{a}} * \underline{\hat{a}}^T\right\} = (H^T * R^{-1} * H)^{-1} \qquad [18]$$

leads to

$$E\left\{\underline{\hat{a}} * \underline{\hat{a}}^T\right\} = \sigma_z^2 * (H^T * H)^{-1}$$

the matrix calculated this way has the following representation

$$E\left\{\underline{\hat{a}} * \underline{\hat{a}}^T\right\} = \begin{Bmatrix} \sigma_{a_0}^2 & r_0 r_1 \sigma_{a_0} \sigma_{a_1} & r_0 r_2 \sigma_{a_0} \sigma_{a_2} \\ r_1 r_0 \sigma_{a_1} \sigma_{a_0} & \sigma_{a_1}^2 & r_1 r_2 \sigma_{a_1} \sigma_{a_2} \\ r_2 r_0 \sigma_{a_2} \sigma_{a_0} & r_2 r_1 \sigma_{a_2} \sigma_{a_1} & \sigma_{a_2}^2 \end{Bmatrix}$$

The entries on the diagonal are the squared standard deviations of the fitted parameters. The others describe the correlation between the fit parameters.

For the standard deviation for the estimated parameters we can write

$$\Delta\underline{\hat{a}} = \begin{pmatrix} \sqrt{\sigma^2{}_{a_0}} \\ \sqrt{\sigma^2{}_{a_1}} \\ \sqrt{\sigma^2{}_{a_2}} \end{pmatrix} \qquad [19]$$

and for the parameters with errors

$$\underline{\hat{a}} \pm \Delta\underline{\hat{a}}$$

If we like the standard deviation of the fit plane at a certain point we must consider the correlation of the standard deviation of the parameters. This is done by using the following formula.

$$\sigma\, z_i^{\,2} = \left[\frac{\partial z}{\partial \underline{a}}\right] * \left[E\left\{\underline{\hat{a}} * \underline{\hat{a}}^T\right\}\right] * \left[\frac{\partial z}{\partial \underline{a}}\right]^T \Bigg|_i \qquad [20]$$

where

$$\left[\frac{\partial z}{\partial \underline{a}}\right]\Bigg|_i$$

is the partial derivation of equation [14] to the parameters $a_i$ at the position $(1\ x_i\ y_i)$

The standard deviation of z depends on the position for which it is calculated.
The behaviour of $\sigma_z$ is shown in Figure 31. For the simple example of a straight line fitted through a cloud of points. The points used for the best fit calculation are generated by adding a standard deviated noise to values taken from a line

$$y = mx + b \qquad [21]$$

With the parameters b= 1, m= 0.1. and a standard deviation for the points of $\sigma_y$=0.075
The estimated parameters and errors for the line are according to eq.[3] and eq.[5]

$$\hat{m} = 0.09 \pm 0.02$$
$$\hat{b} = 1.04 \pm 0.07$$

In Figure 28 the original line (dash dotted) the best fit line (solid) and the confidential region of the fitted line is shown as the points and its error bar.

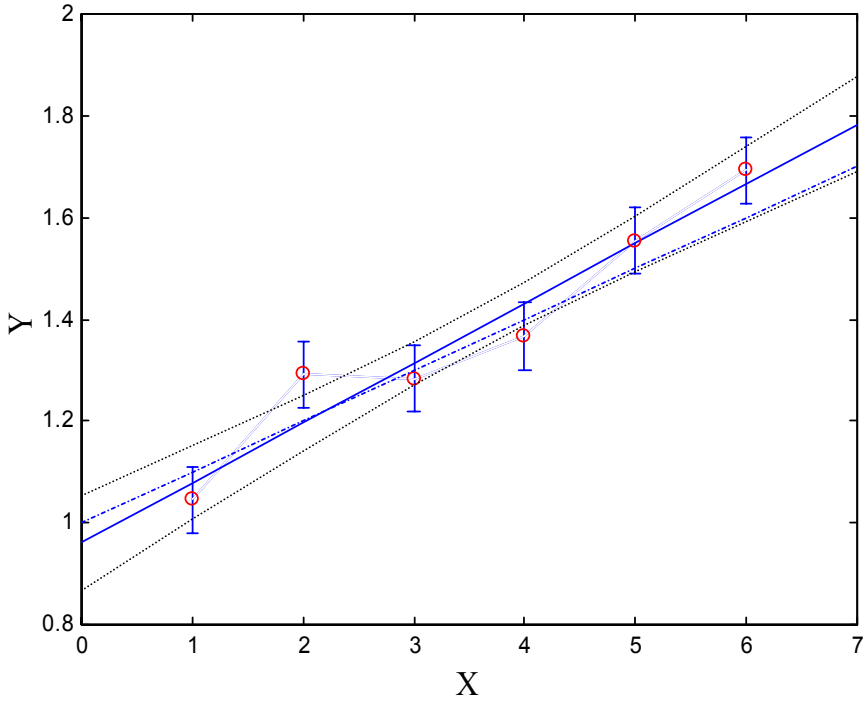


*Figure 28. Confidential interval for a best fit line. For the estimation of the parameters 6 points with a standard deviation of $\sigma_y$=0.075 are used (circles with error bars) The best fit line (solid) is surrounded by the confidential interval (dotted) which marks the region in which the real line is with a probability of 67% . The original solid line (dash dotted) lies inside of this interval.*

The increase of the confidential region of the fitted line near the edge of the interval measured can be depicted as the influence of the number of measured points surrounding the estimated one. This means that a point on the fit line at the edge of the area measured, has only known neighbours in one direction. And is therefore surrounded by less points measured which finally increases the uncertainty for this point on the estimated plane compared to a point at the center of the area measured.

Doing the same calculations for a best fit plane through a 3D cloud of points with a simulated standard deviation of $\sigma_z$ around a given plane and equally distributed over the area of a typical CCD chip of 30mm*60 mm gives the results shown in Figure 29.

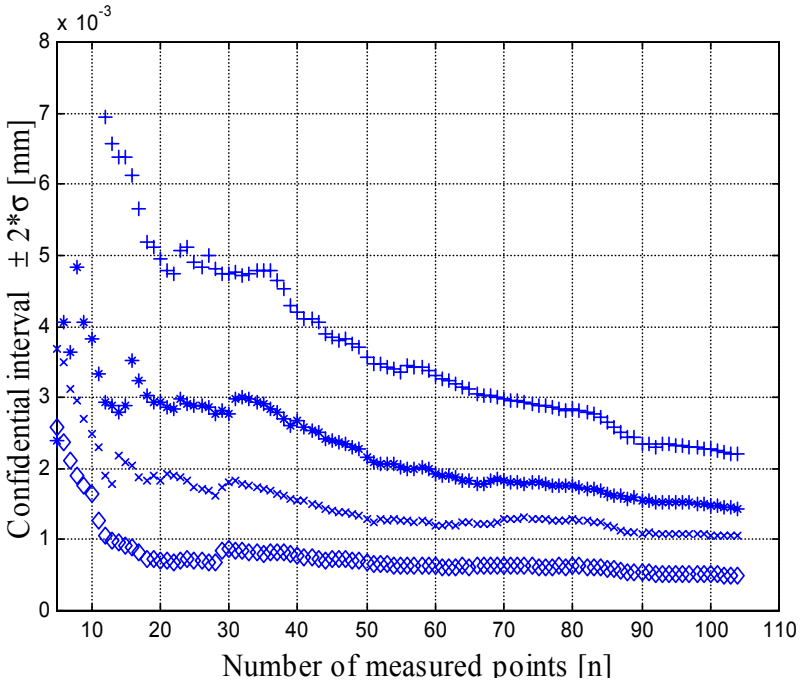


***Figure 29**. 4 σ confidential interval at the corner of a CCD chip for different accuracy simulated of a single measurement: + 8, * 6, x 4, and ◊ 2 microns (4σ). Abszissa number of points used for calculation.*

The rows of plus signs, asterisks, crosses, and diamonds indicate the maximum uncertainty of a least square fit plane determined with n points for one corner of the CCD. The maximum uncertainty in this case means the 4*σ interval calculated by using eq.[7]. Plus signs indicate a measuring device with a accuracy of 8 microns, asterisks one with 6 micron, crosses with 4 micron and diamonds a device with an uncertainty of 2 micron. The course of the markers show roughly a behaviour proportional to 1/sqareroot(n) which is also the behaviour of the average error of the mean.

To achieve the accuracy goal of 2 microns we get different possibilities. We can take only 8 values with a device which is good for 2 microns, around 20 with 6 micron accuracy, more than 60 with 6 micron and some more than 100 with only 8 micron accuracy. The more accurate device will be, the higher its price will be. Taking more than 100 measurements on a single CCD means more than 30000 points for the 16k^2 mosaic will be very time consuming. The best solution in terms of time and costs will be somewhere between.

# 8. Concept and design of the measuring machine.

For an automated measurement of the planarity with a triangulation sensor either the measureing device or the CCD must be moved within the given tolerance. Considering the masses to be moved this decision lies on the hand. The weight of the sensor is with .5 Kg compared with the mass of a whole dewar for a larger mosaic of estimated 50 Kg like a feather. Therefore it will be much easier to position the sensor with micron accuracy than the dewar. Off course both solutions are possible but the machine for moving masses of 50 Kg will easily fill a lab room. Such resources we do not have. So the decision is clear to look further for possibilities for moving the sensor.

The first step in this direction is to check whether there is equipment in house which can be used for this. And the first idea of this is to look weather it is possible to modify the 3D co-ordinate measuring machine for the preliminary measurements. Since this machine was manufactured in 1975 and the company was closed, so there are no documents available describing the electronic access of the positions measured. Additionaly for automation of this machine major changes to the design may be necessary. This may result in a loss of accuracy and functionality. No other adequate solutions are in house, so we have to build or buy one.

## 8.1 Concept

The requirements for such a translation system can be summarised as follows.

- Sufficient accuracy in Z (height).
- No high requirements to the accuracy of the position in X-Y direction (100 micron). It is senseless to demand much there since the laser spot focused onto the surface has a diameter of 100 micron.
- Low speed requirements. To prevent temperature influences for a usage in non air-conditioned rooms a satisfactory result should be acquired within one hour or less
- Affordable in terms of costs and time to realisation.
- Flexible in its usage and easy to handle.

Looking for arrangements providing this I came soon to the following solution. The measuring machine should be a separate device being put upon the camera under test and fixed on it.

A frame providing the translation itself or carrying the movable parts and the sensor is also possible. One commercial solution is provided by Aerotech company. A frame like scanning table can translate quite strong loads within the desired area and accuracy. The weight of 45 kg for a table with 300mm by 300mm shrinks the handling and with 30.000DM the price is out of budget. So lets look whether there are possibilities to design more our self than buy finished devices.

To buy two linear translators screw them together crossed, attach the sensor to one of them and the whole device onto the camera has the disadvantage that one of the linear translator has no support at one side an will suffer from strong flexure under its own

weight. So we have to support the second translator at two points. To do this a part is necessary which can support the linear translator with the same accuracy as the linear translator moves. This is only able if support line and the linear translators are attached to one part. An idea of its shape is shown in Fig. 30.

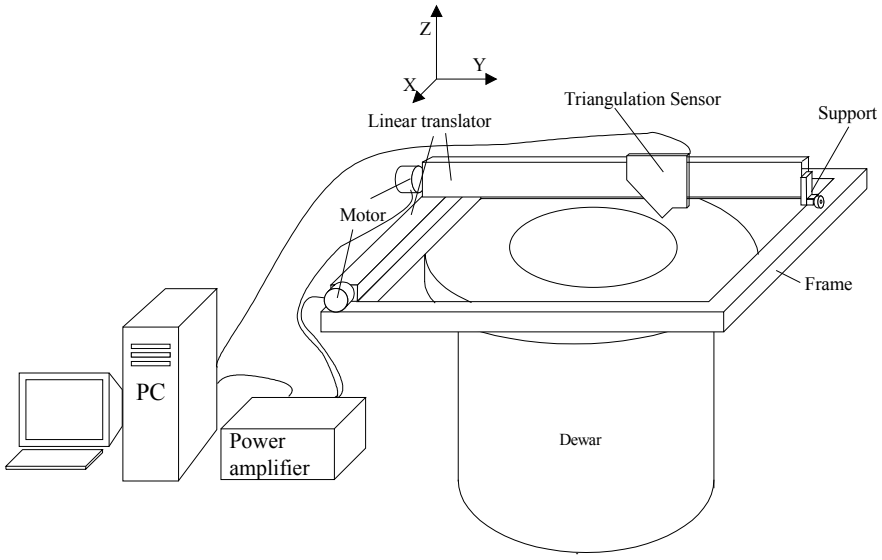


***Figure 30**. Concept for a machine for flatness measurements of CCDs, using a triangulation sensor. The triangulation sensor is attached to a linear translator (Y axis) which itself is attached to a second linear translator providing the movement in X direction. The assembly is supported by a rectangular frame.*

In this case the frame carrying the translators has to take most of the load and must therefore be stiff enough to do this within the specifications. The two translators may then be driven by motors, and a PC takes the control of the stage including the data acquisition.

## 8.2 Mechanical Stage

The critical part of this idea is to achieve good stiffness of the frame without making it very heavy and also the linear translator providing the straightness and repeatability. The frame and linear translator should consist of the same material or at least of one with nearly the same thermal expansion coefficient to prevent a behaviour like a bimetal.

For the linear translators the THK KR33 series or similar can be considered. This system combines sufficient stiffness and precision with small dimensions. They are available with different cross sections, lengths and tolerances.

The stiffness is sufficient to neglect the own flexure of the axis if it is supported at least at two positions. Roughness of movement of the linear translators is not specified for exactly this type, but can be scaled from specifications of similar products and will be below 2 micron.

This means only the roughness of the movement of the sensor in z direction not the influence of remaining flexure. The price of these linear translators is at 3000DM within budget.

***Figure 31**. Linear translator THK-KR33. The moving table is guided by recirculating ball bearings. This table is moved by a ball spindel.*

Having the translation part, now the dimensioning of the frame to which these parts should be attached is considered.

### 8.2.1 Dimensioning of the frame

An important point for the design is the accuracy of the frame which comprise the achievable planarity and the flexure due to the load and its weight under certain circumstances. Additionally the part must be manufactured with conventional effort. In terms of long term accuracy the first choice for the material is grey cast iron. The reason for this is that this material does not have internal stress and thereby will not change its planarity once manufactured after some time. However, for a good stability, tubes have a better weight stiffness proportion. Tubes of grey iron do not exist with suitable dimensions. So we need to find a compromise. Further information for this decision we can get by describing the flexure of the frame analytically and calculate it for different cross sections and materials. This is possible after applying some simplifications and calculate the flexure of the frame for a symmetric part and symmetric load distribution. The frame was split into 4 quarters (Figure 32) and the worst load case was used only. The remaining flexure of the frame under this load will not be zero, but if it is small enough it can be removed. For this a known surface must be measured, e.g. an optical flat, and the systematic deviation of the measurement must be subtracted.

For the modelling I have done the following simplifications:
The frame was cut into 4 symmetric pieces. This can be justified if it is screwed onto the dewar at these 4 points. The cross section at the cut plane does not change since the load is said to be symmetric, both arms of the angle are equally and the connection at the corner is fix. For the load we model a worst case. F is placed at the corner and consists of the own weight of the structure scaled for this point and the maximum load of the moving parts (3.5kg = 7kg/2). The weight of the structure will cause a static deformation, the movable parts instead can cause the whole deformation if they are positioned at the edge of the frame. In this load case to the beams two deformations are applied. The beam gets bent down and the cross section gets twisted. Both kinds of deformation contribute to the rigidity. Adding both contributions we can write for the deformation at the corner

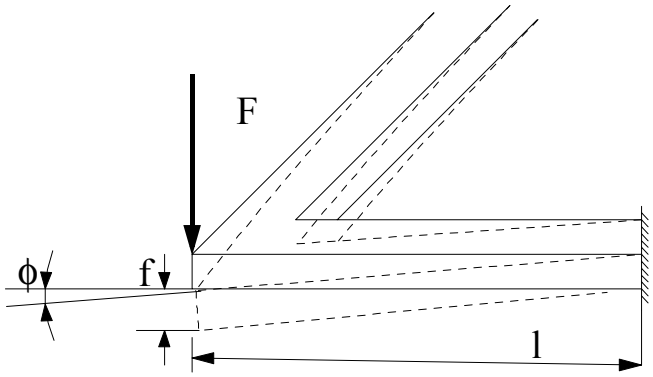


***Figure 32**. Deformation of an angle under a load of F at the position l. f is the depression and Φ the inclination of the beam at the position of l.*

$$f = \frac{F * l^3}{E * I}\left(\frac{1}{3} - \frac{G * I_t}{2 * E * I}\right) \qquad [22]$$

f is counted positive if the flexure goes down, F: Load, l Length of the arm (half of the dimension of the frame) E: modulus of elasticity, G shear modulus, I: second moment of area, $I_t$: second toque momentum of area.

Calculating this deformation for different profiles I found a rectangular tube with a cross section of 50*40mm and a side thickness of 3 mm bends only 12 micron in the worst case and dimensin fits to the linear translator.

U profiles are not very suitable because they are less stable and needs therefore much thicker sides unless the whole frame may be produced in one piece.
The greater stiffness of a tube is the reason for proceeding in this direction and look for an easy solution for the more complicated manufacturing of a frame consisting of rectangular tubes. For the material a stainless steel type 1.4541 was chosen.
For the profile a cross section of 60*40 with 5mm sides was the smallest and thinnest dimension available. For this profile the flexure in the worst case was calculated to 5 microns at the corner. So for measurements on a smaller area in the centre of the structure this flexure can be neglected. The beams can not be connected to a frame by welding, since welding introduces stress into the material. This makes it difficult to achieve afterwards good planarity and keep it over longer periods of time.
To bypass this problem I choose the following solution.

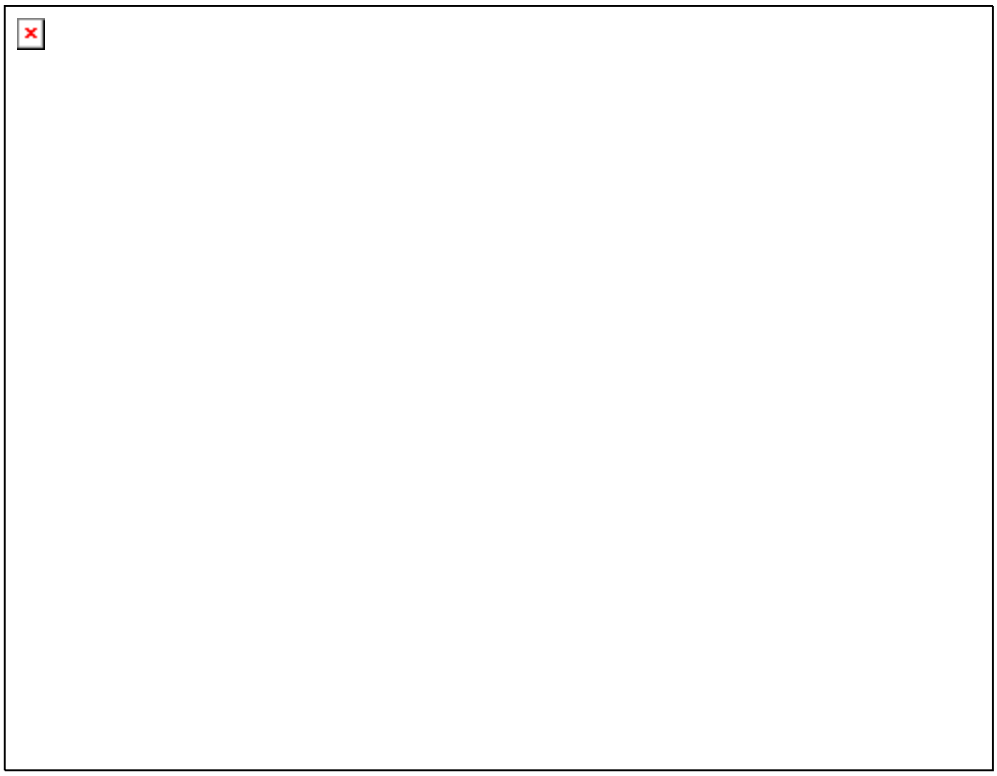

***Figure 33**. Frame which will carry the parts of the measuring machine. To the 4 plates up one linear translator and to the rail a supporting sledge will be attached. To the plates at bottom the flange of the dewar or an adapter will be attached.*

The frame is constructed from of 4 tubes which are connected at the corners by angle pieces and screws. To prevent changes at these connections due to the influence of forces they are additionally fixed with locating pins. To this frame at every point where another part will be connected several plates are attached. The plates allow also a manufacture of the planarity of these points more easily, since material must not be removed from the whole upper and lower surface of the frame and the cross section of the tubes which is essentially responsible for the stiffness gets not reduced.

To the 4 plates on the top one of the linear translators will be screwed, the strip on the opposite side will carry the movable support of the second translator. The plates at the bottom side represent the interface plane to which the dewar flange or any adapter piece between the machine and dewar will be attached. The parts were designed and sketched by me and manufactured according the sketches. For proper documentation later they were redrawn by Guy Hess an industrial designer of ESO. See Appendix C.

After this solution of the mechanical requirements this machine must be automated. This means I have to dimension the drive and find a control system for this task. An automated drive for the measuring machine must contain the following components:

1. Motors for moving the sensor
2. A feedback for recording the position

3. A control unit for device
4. Software as the interface between the user and the machine.

### 8.3 Dimensioning of the Stepper drive.

For the current positioning task, a drive with Stepper motors has a big advantage. Since a stepper motor turns by a certain angle if a digital impulse is applied to it, the position of the motor corresponds to the number of pulses sent to it. The number of pulses must be counted and scaled for the specific application. It is then not necessary to verify the position by a position pick-up and correct the position by a closed loop system. The dimension of the motor must fit very well to the task it has, and there are several critical properties.

The resolution of the positioning is directly connected to the number of steps a motor has per revolution. We require a resolution in X-Y of 100 microns. The spindle of the linear translator has a thread pitch of 6mm (The movable table will be displaced by 6mm if the spindle is turned once around). The number of steps needed per revolution is calculated by

$$number\ of\ steps = \frac{thread\ \ pitch}{resolution} \qquad [23]$$

So we get 60 Steps per revolution. Since there may be a uncertainty of the real position of a stepper motor depending on the load of up to 2 steps we need at least 120 steps per revolution.

The next key dimension is the power and dynamic of the motor. For the measurement in one direction the Sensor and in the other the sensor and one linear translator plus motor must be moved form one point to the next. Therefore its mass must be accelerated and decelerated. Additionally to the power needed for accelerations the friction of the moving parts must be performed by the motor in form of a momentum. In this point a stepper motor is very sensitive. If for example the load of the motor is larger than the torque it can provide it may get stuck. As the only feedback of the position is the count of the steps applied to it, the real position of the motor is lost if the motor does not follow the signal applied to it. Therefore a proper dimensioning of the motor and its drive is essentially.

1. The acceleration is needed, therefore I define the time used for measuring one point to 1 second. Within this time the machine must move the sensor from one position to the next (10mm apart) and leave time for a measurement when the sensor does not move. To fix a number the movement must be completed within 0.4 seconds, the rest of the second is left for measuring this point. So we have to accelerate within 0.2 seconds to a speed of 50mm/s and decelerate the following 0.2 seconds. This gives a acceleration of the driving axle of 260 [rad/s$^2$].

2. The other input is the moment of inertia of the whole load. The linear moved masses must thereby transformed to a moment of inertia. Doing this for the THK KR33 translator with the triangulation sensor we get $13*10^{-6}$ [kg/m$^2$].

An optimum for the energy used for acceleration by stepper motors can be achieved if the momentums of inertia of the load and the motor is equal. So the motor for this drive should fit with this number.
The momentum of friction of the linear axis may be up to 0.15Nm.
After having these numbers we can calculate the load power rate by

$$\dot{P}_L = (J_L * \alpha + M_F) * \alpha * \frac{1}{\eta} \qquad [24]$$

Wherein $J_L$ is the moment of inertia of the load, α is the angular acceleration, $M_F$ is the momentum of friction and η is the efficiency.
The power rate gives growth rate of the power with a unit of W/s .
From this size we can now calculate the momentum needed for acceleration by

$$M_{acc} = \sqrt{P_M * 2 * J_L} \qquad [25]$$

wherein $P_M = 4*P_L$ is the motor power rate.
And by

$$M_{tot} = M_{acc} + M_{load} \qquad [26]$$

we get a total momentum needed for the acceleration of the masses of 0.23 Nm.

Summary of the requirements of the motor:

Number of steps per rev.:120
Momentum of inertia:$13*10^{-6}$ [kg/m$^2$]
Torque at 13rev/s: 0.23Nm

The Zeebotronics company Munich provides a motor fit with 200 steps/rev, inertia of $12.5*10^{-6}$ [kg/m$^2$] and a torque above 0.27Nm, nearly perfect for these requirements. They provide also a driver for this motor, which is in general an amplifier amplifying the digital signal for the speed of the motor generated by the computer enough to move things.
Now we need the interface between the Computer and the power driver. One solution provided by National Instruments. It is the -2OX, PC plug in card controlling 2 stepper motors in an open loop. The PC STEP card generates the signals and frequency profiles for the motors internally. There is also an extended library of functions provided so that the user does not have to do all the low level programming. With this PC plug in card the chain is completed up to a user interface of the PC.

## 8.4 Software

Since I do not now C++ well I have chosen to do this task using LabView from National Instruments for data acquisition and control of the stage and HiQ, an extension for data analysis compatible with Matlab.

At the moment there is only a small part of the software written for testing the stepper motor drive. The connection from LABView to the triangulation sensor via the interface card is done, by calling DDL functions provided by the company selling this device.

For an automated measurement software must be written providing a user interface, the control of the X-Y stage, the data acquisition from the Sensor and an analysis of the data The structure chart below gives an overview.

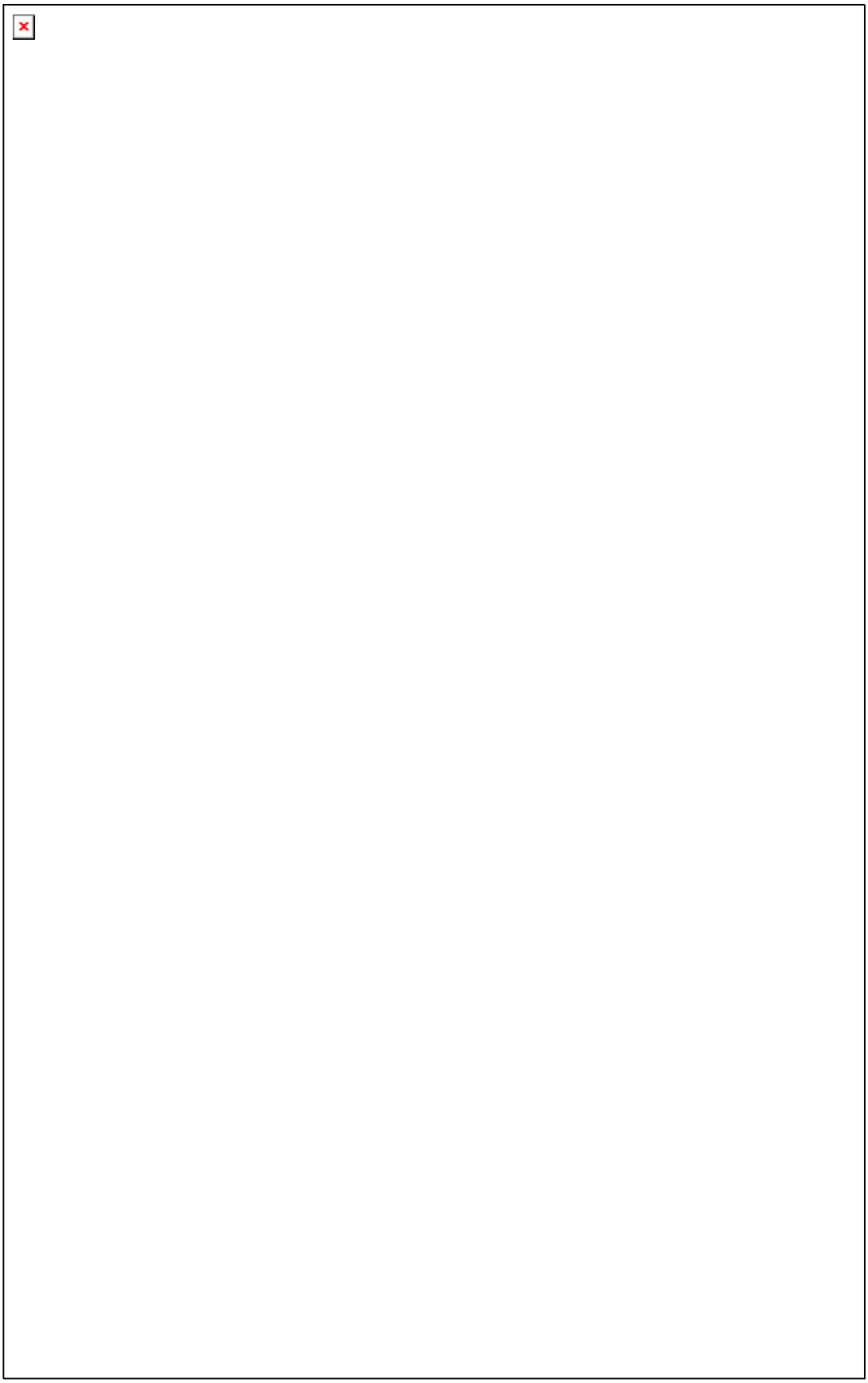

# 9. State of the project at the end of the Diplomarbeit

The measuring machine is not completed yet. Up to now all the mechanical parts are ordered but not all are manufactured. The driver system consisting of the Stepper motor card, amplifier, stepper motors and linear translators is assembled and tested. Also the triangulation sensor can be driven and the measured values acquired by a PC. A suite of programmes was written to demonstrate this.

It remains to assemble and align all the parts and write the software for running the machine and analysing the data.

# 10. Conclusion

By the time I had to hand in this degree dissertation I had found a means of measuring the flatness of CCDs, and mosaics of them. I proved that a triangulation sensor commercially available can be used for this task and gained experience in using them. A device providing an automated measurement was designed, dimensioned and nearly completed.

This measuring machine will allow ESO a fast measurement of the flatness of CCDs and mosaics of CCDs with a size of 310 by 330 mm with an accuracy of few microns.

# Appendix A

## Deflection of a light beam on its path through a optical flat.

If a light beam passes an optical flat not perpendicular to it, it gets refracted two times, when it enters the glass and when it exits the glass. As long as the medium on both sides of the window has the same index of refractivity the beam gets two times refracted by the same angle with different orientation. So it gets a parallel offset.
In Figure A1 the beam path is shown.

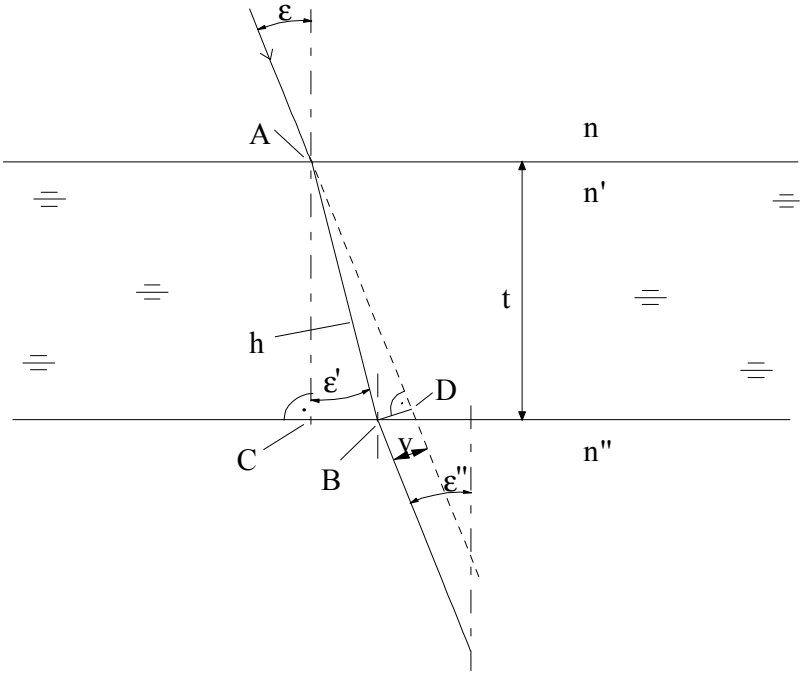


*Figure A1. Parallel offset of a beam after its transit of an optical flat.*

For the case of having the same medium on both sides of the optical flat two simplifications are possible.

$n'' = n$ and $\varepsilon'' = \varepsilon$

The offset of the beam can then be calculated by using a help size *h* which is the geometric path length of the light inside the glass. We can write for the triangle A C B

$$\frac{t}{h} = \cos\varepsilon' \qquad [A1]$$

And for A B D

$$\frac{v}{h} = \sin(\varepsilon - \varepsilon') \qquad [A2]$$

by using Snell's law

$$n * \sin\varepsilon = n' * \sin\varepsilon'$$

And

$$\sin(\varepsilon - \varepsilon') = \sin\varepsilon * \cos\varepsilon' - \cos\varepsilon * \sin\varepsilon'$$

follows for the parallel offset of the beam v

$$v = t * \sin\varepsilon \left( 1 - \frac{\cos\varepsilon}{\sqrt{\left(\frac{n'}{n}\right)^2 - \sin^2\varepsilon}} \right) \qquad [A3]$$

V depends on the thickness of the window t, the inclination of the incoming beam and the index of refractivity.

# Appendix B

## Matlab functions used for data analysis.

For the analysis of the points measured as set of functions were written in Matlab. This simplifies the analysis since more complicated formulas repeating several times must not be written and debugged in every case they are used. Beside this functions I give an example of how an analysis of a certain set of measurements is done. The listing for the simulation of the influence of the error of a single measurement is also attached.

## Matlab functions

**(par) fitplane (values) :**

input values: values: Vector with 3*n entries, the values 1-n must be the x co ordinates,
the values (n+1) to (2*n) the Y co ordinates and
the values (2*n+1) to (3*n) the Z co ordinates.

Return values: par: A vector conpainig the estimated parameters of plane determined by a least square algorithm according the formula

$$z = a_0 + a_1 x + a_2 y$$

Listing:

```
% fit of the least square plane
%at a set of measurements.
%returns a vector of parameters
%z=a1+a2*x+a3*y

function [par]=fitplane(values)
d=size(values);
h1=ones(d(1),1);
x=values(1:d(1));
y=values(d(1)+1:2.*d(1));
z=values(2.*d(1)+1:3.*d(1));
H=[h1,x',y'];
par=((inv(H'*H))*H'*z');
```

**pplane (values,par):**

input values values: Vector with 3*n entries, the values 1-n must be the x co ordinates,
the values (n+1) to (2*n) the Y co ordinates and
the values (2*n+1) to (3*n) the Z co ordinates.

par: A vector containing the parameters of a plane according the formula

$$z = a_0 + a_1 x + a_2 y$$

Return: Graph of a plane with the parameters par on the area claimed by values.
( useful for plotting the tilts of single CCDs in a mosaic. )

listing:

```
function pplane(values,par)
%plots a plane with the parameters par
%on the range of values
d=size(values);

% splitting off of the values in x,y,z co ordinates
x=values(1:d(1));
y=values(d(1)+1:2.*d(1));
z=values(2.*d(1)+1:3.*d(1));
% determination of the area
dx=max(x)-min(x);
dy=max(y)-min(y);
xi=(min(x):(dx/10):max(x));
yi=(min(y):(dy/10):max(y));
% creation of a regular grid on this area
[XI,YI] = meshgrid(xi,yi);
ZI=(par(1)+par(2).*XI+par(3).*YI);
% plotting
surf(XI,YI,ZI);
```

**(rmserror,pp) fitqual (values,par)**

input values values: Co ordinates of points. Vector with 3*n entries, the values 1-n must be the x co ordinates,
the values (n+1) to (2*n) the Y co ordinates and
the values (2*n+1) to (3*n) the Z co ordinates.

par: A vector containing the parameters of a plane according the formula
$z = a_0 + a_1 x + a_2 y$

Return: rmserror: rms value of the distances of the points defined by values to the plane defined by par

pp: Peak to valley distance of the points defined by values to the plane defined by par

Listing

```
function [rmserror,pp]=fitqual(values,par)
d=size(values);

% splitting off of the values in x,y,z co ordinates
x=values(1:d(1));
y=values(d(1)+1:2.*d(1));
z=values(2.*d(1)+1:3.*d(1));
%calculation of the distancee point-plane
dz=z-(par(1)+par(2).*x+par(3).*y);
rmserror=sqrt(((dz*dz')/d(1)));
pp=max(dz)-min(dz);
```

Typical listing for analysing a set of measurements of UVES red, a mosaic of two different CCDs

```
%Corrections for the mosaic of UVES red based on my measurement from
%18.11.98
'Analysis of measurement Nr. 9'
% loading of the data stored in text files
load muevmi9.txt
load muwin9u.txt
chippoi=muevmi9;
refpoi=muwin9u;

'Analysis of both chips together Chips'
chippar=fitplane(chippoi)
 [rms,pv]=fitqual(chippoi,chippar);
rms
pv

'Analysis of the window back side'
winpar=fitplane(refpoi)
 [rms,pv]=fitqual(refpoi,winpar);
rms
pv

'Analysis of the EEV chip'
load mueev9.txt;
eevpar=fitplane(mueev9)
[rms,pv]=fitqual(mueev9,eevpar);
rms
pv

'Analysis of the MIT chip'
load mumit9.txt;
mitpar=fitplane(mumit9)
[rms,pv]=fitqual(mumit9,mitpar);
rms
pv

'Deviation of the Chips relative to the best fit-plane of the window'
%Creation of a new vector winpar with the tilt of winpar
%and the offset of chippar
tiltpar=[chippar(1) winpar(2) winpar(3)];
[rms,pv]=fitqual(chippoi,tiltpar');
rms
pv

% Display of the surface of the CCDs and the reference
disp2pla(refpoi,chippoi)
hold off

% definition of the points of correction on EEV CCD
p1=[1 23 33];p2=[1 23 55];p3=[1 62 44];
```

```
% Calculation of the corrections to be applied to the shims
supporting %the EEV CCD to get both CCDs aligned best possible

'MIT as reference, corrections on EEV'
eev1=[p1*eevpar p2*eevpar p3*eevpar];
mit1=[p1*mitpar p2*mitpar p3*mitpar];
eev1-mit1

%Analysis of the CCDs relative to the reference plane
'MIT chip relative to the best fit plane of the window'
mtiltpar=[mitpar(1) winpar(2) winpar(3)];
[rms,pv]=fitqual(mumit9,mtiltpar');
rms
pv

'EEV chip relative to the best fit plane of the window'
etiltpar=[eevpar(1) winpar(2) winpar(3)];
[rms,pv]=fitqual(mueev9,etiltpar');
rms
pv
```

Listing written for the simulation of the influence of the error of a single point measured to the accuracy of the fit plane.

```
% simulation of the influence of the error of a single measurement
% and its number on the remaining error of a least square fitted
plane.
%
Generation of an array of points
nmin=5;
nmax=110;
imax=100;
xsize=60;
ysize=30;
sig_m=[ 0.002 0.0015 0.001 0.0005];
%Different standard deviations of the measurement
par=[.1 .01 .01];% parameters of the original plane
linest=['+' '*' 'x' 'diamond'];% symbols for plotting
cpoint=[1 60 30];%point for which the error is simulated (at a
corner)

%creation of points randomly distributed in the field analysed with
%normal distributed values in z
 xmax=rand(nmax,1)*xsize;
 ymax=rand(nmax,1)*ysize;
 h1max=ones(1,nmax);
 e1=sprandn(xmax)*sig_m;
 emax=e1(1:nmax);
% for loop for the 4 different cases of standard dviation of a sinle
%point
for j=1:4
  e1=sprandn(xmax)*sig_m(j);
  emax=e1(1:nmax);
  n=nmin;
  % for loop for the calculation of the error when the number of
   points
  % used for the calculation is increasing.
  for i=1:imax
   x=xmax(1:n);% selection of a field wit n by n points
   y=ymax(1:n);
   h1=h1max(1:n);% creation of a vector containing n times 1
   H=[h1',x,y];
   z=par*H';
   e=emax(1:n);%selection of n normal distributed values
   ze=z+e'; % creation of the noisy points around a plane
   parest=(inv(H'*H))*H'*ze'; % determination of the parameters of
      %the plane ( least square according the formula z=a0+a1*x+a2*y
   sigma(i)=std(e); % det. of the real st deviation
   E=sigma(i)^2*inv(H'*H);% covariance matrix
   cin=cpoint*E*cpoint';
   cint(i)=sqrt(cin); %standard error of the plane determined at
                         %the position of cpoint
   zsigsq=H*E*H';
   v = diag(zsigsq);
   zsig=sqrt(v);% standard error for the estimated parameters
```

```
   m(i)=max(zsig);
   index(i)=n;
   n=nmin+i;
  end;% end of for
  si=size(cint);
  %plot of the results
  plot(index(1:imax),4.*cint(1:imax),linest(j));
  hold on
  xlabel('Number of measured points
[n]','FontSize',14,'FontName','Times New Roman');
  ylabel('Confidential interval   \pm 2*\sigma
[mm]','FontSize',14,'FontName','Times New Roman');

end;
axis([nmin nmax 0 0.008]);

grid on
hold off
```

# Appendix C

**Drawings.**

In the following I attach the drawings for the parts specially manufactured for the measure machine with following order.

1. Axonometric charts of top and bottom view of the assembled frame
2. Top and bottom view of the assembled frame
3. Bar 1 (part 01)
4. Bar 2 (part 02)
5. Bar 3 (part 03)
6. Corner (part 05/06)
7. Spacer plate up (part 07)
8. Spacer plate up (part 08)
9. Spacer plate down (part 09)
10. Guiding part (part 10)

For the assembly of the linear translators, and motors the following parts were manufactured:

11. Plate 1 (part 15)
12. Plate 2 (part 16)
13. Plate 3 (part 17)
14. Plate 4 (part 18)
15. Plate 5 (part 19)
16. Coupling (part 20)
17. Plate 6 (part 21)
18. Flange (part 22)